GE Energy

Robert E. Gamble
Manager, ESBWR

175 Curtner Ave. M/C 365
San Jose, CA 95125-1014
USA

T 408 925 3352
F 408 925 5665
Robert.gamble@ge.com

MFN 04-140

Project 717

December 22, 2004

U.S. Nuclear Regulatory Commission
Document Control Desk
Washington, D.C. 20852-2738

Subject: **Licensing Topical Report, "TRACG Application for ESBWR Stability Analysis," NEDO-33083, Supplement 1, December 2004**

Enclosure 1 contains the subject licensing topical report. This document is the non proprietary version of NEDE-33083P, Supplement 1, which was transmitted to the NRC via the referenced letter.

If you have any questions about the information provided here, please let me know.

Sincerely,

Robert E. Gamble
Manager, ESBWR

D068

Reference:

1. MFN 04-131, Letter from Robert E. Gamble to U.S. Nuclear Regulatory Commission, *Submittal of Licensing Topical Report, "TRACG Application for ESBWR Stability Analysis," NEDE-33083P, Supplement 1, December 2004*, December 9, 2004

Enclosure:

1. MFN 04-140 – NEDO-33083, Supplement 1, TRACG Application for ESBWR Stability Analysis, Licensing Topical Report

cc: WD Beckner USNRC (w/o enclosures)
AE Cubbage USNRC (with enclosures)
MB Fields USNRC (with enclosures)
GB Stramback - GE (with enclosures)
eDRF-0000-0030-1246

ENCLOSURE 1

MFN 04-140

NEDO-33083, Supplement 1
TRACG Application for ESBWR Stability Analysis
Licensing Topical Report
December 2004

GE Nuclear Energy

175 Curtner Ave., San Jose, CA 95125

NEDO-33083
Supplement 1
eDRF-0000-0030-1246
Class I
December 2004

LICENSING TOPICAL REPORT

TRACG APPLICATION FOR ESBWR STABILITY ANALYSIS

B. S. Shiralkar
L. A. Klebanov
Y. K. Cheung

Approved : R. E. Gamble,
Manager, ESBWR

IMPORTANT NOTICE REGARDING CONTENTS OF THIS REPORT PLEASE READ CAREFULLY

The information contained in this document is furnished for the purpose of obtaining NRC approval of the licensing requirements for implementation of the stability Detect and Suppress Solution – Confirmation Density (DSS-CD) to provide automatic detection and suppression of stability related power oscillations. The only undertakings of General Electric Company with respect to information in this document are contained in contracts between General Electric Company and participating utilities, and nothing contained in this document shall be construed as changing those contracts. The use of this information by anyone other than that for which it is intended is not authorized; and with respect to **any unauthorized use**, General Electric Company makes no representation or warranty, and assumes no liability as to the completeness, accuracy, or usefulness of the information contained in this document.

TABLE OF CONTENTS

Acknowledgements ix
Acronyms and Abbreviations x
1.0 Introduction 1-1
1.1 Background 1-1
1.2 Purpose and Scope 1-1
1.3 Scope of Review 1-3
2.0 Licensing Requirements and Scope of Application 2-1
2.1 Licensing Compliance 2-1
2.2 Stability Design Criteria 2-1
2.3 TRACG Analysis Approach For Licensing Compliance 2-5
2.3.1 Conformance with CSAU Methodology 2-5
2.4 Implementation Requirements 2-9
2.4.1 Review Requirements For Updates 2-9
2.5 Range of Application 2-9
3.0 Phenomena Identification And Ranking 3-1
3.1 ESBWR Stability PIRT 3-1
4.0 Applicability of TRACG To ESBWR Stability Analysis 4-1
4.1 Model Applicability 4-1
4.2 Assessment Matrix 4-1
4.3 Other Topics Relevant To TRACG Modeling of Instability 4-12
4.3.1 Explicit Integration Scheme for the Channel Component 4-12
4.3.2 Coupling of Conduction and Hydraulic Equations 4-12
4.3.3 Coupling of the Vessel and Channel Components 4-13
4.3.4 Coupled 3-D Kinetics and Thermal-Hydraulics Model 4-13
4.4 TRACG Qualification against Peach Bottom Unit 2 Stability Data 4-15
4.4.1 Test Conditions and Test Results 4-15
4.4.2 TRACG Analysis 4-15
4.4.3 Sensitivity Studies 4-16
4.4.4 Channel Decay Ratio 4-16
5.0 Model Biases and Uncertainties 5-1
5.1 Model Parameters and Uncertainties 5-1
5.2 Effects of Nodalization 5-20
5.2.1 Vessel Nodalization for ESBWR Stability Analysis 5-20
5.2.2 Detailed Nodalization Scheme for the Channel Component 5-20
5.2.3 Channel Grouping for Stability Applications 5-21
5.3 Effects of Scale 5-27
5.3.1 Full Scale Test Coverage 5-27
5.3.2 Operating Plant Data 5-27
5.4 Sensitivity Analysis 5-31
6.0 Application Uncertainties and Biases 6-1
6.1 Key Initial Conditions and Plant Parameters 6-1
7.0 Combination of Uncertainties 7-1

7.1 Traditional Bounding Analysis 7-1
7.2 Statistical Treatment of Overall Calculational Uncertainty 7-1
7.3 Comparison of Approaches for Combining Uncertainties 7-2
7.3.1 Propagation of Errors 7-3
7.3.2 Response Surface Technique 7-3
7.3.3 Order Statistics (OS) Method – Single Bounding Value 7-4
7.3.4 Normal Distribution One-Sided Upper Tolerance Limit 7-6
7.4 Recommended Approach for Combining Uncertainties 7-6
7.5 Implementation of Statistical Methodology 7-9
7.5.1 Conformance with Design Limits 7-9
8.0 Demonstration Analyses 8-1
8.1 Baseline Analysis 8-1
8.1.1 Channel Stability Results 8-2
8.1.2 Core wide Stability Results 8-3
8.1.3 Regional Stability Results 8-4
8.2 Sensitivities to High and Medium Ranked Parameters 8-25
8.2.1 Channel Decay Ratio 8-25
8.2.2 Core Decay Ratio 8-25
8.3 Statistical Analysis of ESBWR Stability 8-29
8.3.1 Channel Decay Ratio Statistical Analysis 8-29
8.3.2 Core Wide Decay Ratio Statistical Analysis 8-30
8.3.3 Comparison with Design Limits 8-30
8.4 Stability following Anticipated Operational Occurrences (AOOs) 8-37
9.0 Plant Startup 9-1
9.1 Phenomena Governing Oscillations during Startup 9-1
9.2 Applicability of TRACG for Startup Calculations 9-6
9.3 TRACG Analysis of Typical Startup Trajectories 9-9
9.3.1 ESBWR Plant Startup 9-9
9.3.2 TRACG calculations for Simulated Startup Scenarios 9-9
9.4 Summary of ESBWR Startup Performance 9-19
10.0 References 10-1

LIST OF TABLES

Table 2.3-1: Code Scaling, Applicability and Uncertainty Evaluation Methodology 2-8
Table 3.1-1: Phenomena Governing ESBWR Stability Transients 3-4
Table 3.1-2: Initial Conditions and Plant Parameters 3-8
Table 4.2-1: Stability Phenomena and TRACG Model Capability Matrix 4-3
Table 4.2-2: Qualification Assessment Matrix for High and Medium Ranked ESBWR Stability Phenomena 4-8
Table 4.4-1: PB2 Operating Conditions for Stability Tests 4-17
Table 4.4-2: PB2 Stability Test Results 4-17
Table 4.4-3: TRACG Channel Grouping for PB2 Core 4-17
Table 4.4-4: Comparison of TRACG Predictions with Test Data 4-18
Table 4.4-5: Sensitivity to Applied Perturbations 4-18
Table 5.1-1: Bias and Uncertainty in Pressure Drop for 9x9 and 10x10 SEO and Lower Tie Plates 5-12
Table 5.1-2: Bias and Uncertainty in Pressure Drop for 9x9 and 10x10 Spacers 5-12
Table 5.1-3: Bias and Uncertainty in Pressure Drop for 9x9 and 10x10 Upper Tie Plates 5-13
Table 5.1-4: Disposition of High and Medium Ranked Stability Model Parameters 5-18
Table 5.2-1: Void Distribution at the Top of the Bypass Region 5-23
Table 5.3-1: Range of Key Stability Parameters - ESBWR vs. Operating Plant Data 5-29
Table 6.1-1: Key Plant Initial Conditions 6-2
Table 7.3-1: Methods for Combining Uncertainty 7-2
Table 7.4-1 Comparisons of Methods for Combining Uncertainties 7-8
Table 8.1-1: TRACG Channel Grouping 8-6
Table 8.1-2: Higher Harmonic Mode Sub-criticality at Different Exposures 8-7
Table 8.1-3: Initial Conditions for Channel and Core Stability Analysis 8-7
Table 8.1-4 Initial Conditions for Super Bundle Stability Analysis 8-8
Table 8..1-5: Regional Stability: Decay Ratio by Subgroup 8-8
Table 8.2-1: Sensitivity of Channel Decay Ratio to High and Medium-Ranked PIRT Parameters 8-27
Table 8.2-2: Sensitivity of Core Decay Ratio to High and Medium-Ranked PIRT Parameters 8-28
Table 8.3-1: Parameters and Distributions for Monte Carlo Trials 8-32

Table 9.2-1: Comparison of Non-dimensional Parameters: CRIEPI vs. ESBWR 9-8
Table 9.2-1: Comparison of Non-dimensional Parameters: Dodewaard vs. ESBWR 9-8

LIST OF ILLUSTRATIONS

Figure 2.2-1: Stability Acceptance Criteria for BWRs 2-3
Figure 2.2-2: Proposed Stability Map for ESBWR 2-4
Figure 3.1-1: Schematic of ESBWR Vessel and Internals 3-9
Figure 3.1-2: Top View of ESBWR Chimney and Core Region 3-10
Figure 4.3-1: Data Transfer Between TRACG Models 4-14
Figure 4.4-1: Test Conditions on PB2 Power/Flow Map 4-19
Figure 4.4-2: Average Axial Power Shapes for Stability Tests 4-19
Figure 4.4-3: Power Response to Pressure Perturbation for Test PT1 4-20
Figure 4.4-4: Power Response to Pressure Perturbation for Test PT2 4-20
Figure 4.4-5: Power Response to Pressure Perturbation for Test PT3 4-21
Figure 4.4-6: Power Response to Pressure Perturbation for Test PT4 4-21
Figure 4.4-7: TRACG Predictions of Decay Ratio versus Data 4-22
Figure 4.4-8: Sensitivity to Core Flow Perturbation Amplitude 4-22
Figure 4.4-9: Sensitivity to Number of Channel Groups (Test PT2) 4-23
Figure 4.4-10: Channel Decay Ratio for Test PT3 4-23
Figure 5.1-1: TGBLA06 Void Coefficient Relative Bias and Relative Standard Deviation for Various Exposures (GWd/MT) 5-4
Figure 5.1-2. FRIGG OF64 Void Fraction Data – Subcooled Boiling 5-7
Figure 5.1-3. Void Fraction Sensitivity to PIRT23 5-7
Figure 5.1-4. Sensitivity of Fuel Center to Fluid Temperature Difference for 8x8 Fuel 5-9
Figure 5.1-5. Sensitivity of Fuel Center to Fluid Temperature Difference for 9x9 Fuel 5-9
Figure 5.1-6. Void Fraction Deviations for Tests Applicable to Regions with Large Hydraulic Diameter 5-15
Figure 5.1-7. Sensitivity of TRACG Prediction of Average Void Fraction in EBWR Test Facility to PIRT Multiplier on Interfacial Drag Coefficient 5-16
Figure 5.1-8 Probability Distribution for Multiplier on Interfacial Drag Coefficient 5-16
Figure 5.2-1: Axial and radial nodalization for ESBWR Stability Analysis 5-24
Figure 5.2-2: Channel Nodalization Studies from Reference 2 5-25
Figure 5.2-3: R- θ Nodalization for ESBWR Stability Analysis 5-25
Figure 5.2-4: Channel Grouping for ESBWR Stability Analysis 5-26

Figure 5.3-1: Comparison of Power and Flow per Bundle for ESBWR vs. Operating BWRs5-30
Figure 5.3-2: Variation in Harmonic Sub-criticality vs. Core Size 5-30
Figure 7.3-1. Schematic Process for Combining Uncertainties 7-5
Figure 8.1-1. TRACG ESBWR Vessel R-Z Modeling 8-9
Figure 8.1-2: R-θ Nodalization of ESBWR Core Region showing Average Power (MW) in Each Region 8-10
Figure 8.1-3: TRACG Channel Grouping for ESBWR Core 8-11
Figure 8.1-4: Core Average Axial Power Shape at Different Exposures 8-12
Figure 8.1-5: Flux Distribution for First Azimuthal Harmonic with Axis of Symmetry 8-13
Figure 8.1-6: Flux Distribution for Second Azimuthal Harmonic with Axis of Symmetry ... 8-14
Figure 8.1-7: ESBWR Natural Circulation Operation with Limiting Conditions for Stability Analysis 8-15
Figure 8.1-8: Hot Bundle Flow Response to Transient Inlet Flow Perturbation 8-16
Figure 8.1-9: Hot Super Bundle Flow Response to Transient Inlet Flow Perturbation 8-16
Figure 8.1-10: Core Power Response to Transient Turbine Inlet Pressure Perturbation 8-17
Figure 8.1-11: Sensitivity to Perturbation Size 8-17
Figure 8.1-12: Power Distribution by Channel in Large Sectors in Ring 1 8-18
Figure 8.1-13: Power Distribution by Channel in Large Sectors in Ring 2 8-18
Figure 8.1-14: Finer Channel Grouping by Power Level 8-19
Figure 8.1-15: Sensitivity to Detailed Channel Grouping 8-20
Figure 8.1-16: Power Distribution for First Harmonic 8-21
Figure 8.1-17: Core Map showing Products of Fundamental and First Harmonic Powers (Regions with highest values are shown in dark brown) 8-22
Figure 8.1-18: Channel Grouping for Regional Stability Calculation (darker colored regions have higher absolute peaking) 8-23
Figure 8.1-19: Channel Power Responses to Out-of-Phase Flow Perturbation 8-24
Figure 8.1-20: Symmetrically Located Channel Power Responses to Out-of- Phase Flow Perturbation 8-24
Figure 8.3-1: Monte Carlo Trials for Channel Decay Ratio 8-33
Figure 8.3-2: Monte Carlo Results for Channel Flow 8-33
Figure 8.3-3: Monte Carlo Results for Channel Decay Ratio 8-34
Figure 8.3-4: Monte Carlo Trials for Core Decay Ratio 8-34
Figure 8.3-5: Correlation between Core Decay Ratio and Power/Flow Ratio 8-35

Figure 8.3-6: Monte Carlo Results for Core Flow 8-35
Figure 8.3-7: Monte Carlo Results for Core Decay Ratio 8-36
Figure 8.3-8: Decay Ratio Results Compared to Design Criteria 8-36
Figure 8.4-1: Stability in Expanded Operating Map 8-39
Figure 8.4-2: Loss of Feedwater Heater Transient 8-39
Figure 8.4-3: Core Power Response to Pressure Perturbation 8-40
Figure 8.4-4: Hot Channel Flow Response to Inlet Flow Perturbation 8-40
Figure 8.4-5: Core Power Response to Pressure Perturbation at Reduced Level 8-41
Figure 8.4-6: Hot Channel Response to Inlet Flow Perturbation at Reduced Level 8-41
Figure 9.1-1: Generalized Stability Map showing Type 1 and Type 2 Instability [28] 9-4
Figure 9.1-2: Indications of Periodic Behavior during Dodewaard Startup [29] 9-4
Figure 9.1-3: Thermal – Hydraulic Conditions during Startup [28] 9-5
Figure 9.1-4: Enthalpy Profiles for Different Heatup Rates 9-5
Figure 9.3-1: ESBWR Startup Trajectory 9-11
Figure 9.3-2: ESBWR Reactor Water Cleanup/Shutdown Cooling System – Schematic Diagram 9-11
Figure 9.3-3: TRACG Startup Simulation: Reactor Power Trajectories 9-12
Figure 9.3-4: TRACG Startup Simulation: Pressure Response 9-12
Figure 9.3-5: TRACG Startup Simulation – Core Inlet Subcooling 9-13
Figure 9.3-6: TRACG Startup Simulation – Core Inlet Flow 9-13
Figure 9.3-7: Separator Void Fraction (50 MW heatup) 9-14
Figure 9.3-8: Separator Void Fraction (85MW heatup) 9-14
Figure 9.3-9: Separator Void Fraction (125 MW heatup) 9-15
Figure 9.3-10: Hot Bundle Void Fraction (50 MW heatup) 9-15
Figure 9.3-11: Hot Bundle Void Fraction (85 MW heatup) 9-16
Figure 9.3-12: Hot Bundle Void Fraction (125 MW heatup) 9-16
Figure 9.3-13: Hot Bundle Exit Flow 9-17
Figure 9.3-14: Peripheral Bundle Exit Flow 9-17
Figure 9.3-15: Hot Bundle CPR 9-18
Figure 9.3-16: Peripheral Bundle CPR {3}]] 9-18

ACKNOWLEDGEMENTS

The following individuals contributed significantly to the development, verification, and review of this report:

J. C. Shaug

W. Marquino

R. B. Linford

A. Chung

J. G. M. Andersen

C. L. Heck

ACRONYMS AND ABBREVIATIONS

Term	Definition
AOO	Anticipated Operational Occurrence
BOC	Beginning of cycle
BT	Boiling Transition
BWR	Boiling Water Reactor
CCFL	Counter Current Flow Limitation
CHAN	Fuel Channel component in TRACG
CPR	Critical Power Ratio
CSAU	Code Scaling, Applicability and Uncertainty
DSS-CD	Detect and Suppress Solution – Confirmation Density
DVC	Dynamic Void Coefficient
ECCS	Emergency Core Coolant System
EOC	End Of Cycle
ESBWR	Economic Simplified Boiling Water Reactor
FTTC	Fuel Thermal Time Constant
FW	Feedwater
FWTR	Feedwater temperature reduction
GDC	General Design Criteria
GESTAR	General Electric Standard Application for Reload Fuel
GEXL	GE Boiling Transition Correlation
GT	Guide Tube
H	High Importance
HT	Heat Transfer
ICPR	Initial Critical Power Ratio
L	Low Importance
LOCA	Loss Of Coolant Accident
LTP	Lower Tieplate
LTR	Licensing Topical Report
M	Medium Importance
MCPR	Minimum Critical Power Ratio
MOC	Middle Of Cycle
NA	Not Applicable
NRC	Nuclear Regulatory Commission

Term	Definition
OLMCPR	Operating Limit MCPR
PANAC11	PANACEA, GE BWR Core Simulator
PIRT	Phenomena Identification and Ranking Table
PHE	Peak Hot Excess
RFACT	R Factor
SAFDL	Specified Acceptable Fuel Design Limit
SEO	Side entry orifice
TRACG	Transient Reactor Analysis Code (GE proprietary version)
UTP	Upper Tieplate
1-D	One Dimensional
1P	Single Phase Pressure Drop
2P	Two Phase Pressure Drop
3-D	Three Dimensional

1.0 INTRODUCTION

1.1 BACKGROUND

Under certain conditions, Boiling Water Reactors (BWRs) may be susceptible to coupled neutronic/thermal-hydraulic instabilities. These instabilities are characterized by periodic power and flow oscillations and are the result of density waves (i.e., regions of highly voided coolant periodically sweeping through the core). If the flow and power oscillations become large enough, and the density waves contain a sufficiently high void fraction, the fuel cladding integrity safety limit could be challenged.

Operating BWRs are implementing detection and mitigation solutions such as Detect and Suppress Solution – Confirmation Density (DSS-CD) [4]. These solutions consist of hardware and software that provide for reliable, automatic detection and suppression of stability related power oscillations, in the event that these plants enter the low flow region of the operating map. In the Economic Simplified Boiling Water Reactor (ESBWR), the highest power to flow ratio (and hence the smallest stability margin) is encountered at rated operation. Thus, it is essential that the ESBWR operate with substantial margin to instability at rated power. This requirement is met by imposing very conservative design criteria on the decay ratio. Detect and Suppress solutions will also be implemented, but only to serve as a backup in the very unlikely event that oscillations are encountered.

The TRACG computer code is used for the analysis of ESBWR stability margins. TRACG is a General Electric (GE) proprietary version of the Transient Reactor Analysis Code (TRAC). TRACG uses advanced one-dimensional and three-dimensional methods to model the phenomena that are important in evaluating the operation of BWRs. TRACG has been approved by the NRC for ESBWR LOCA (ECCS and containment) analysis. [24]. The application of TRACG for Anticipated Operational Occurrences (AOOs) and for ATWS overpressure calculations for operating BWRs has also been approved by the NRC [3], [31]. Currently, the NRC is reviewing the use of TRACG for BWR stability analysis in connection with the DSS-CD application [5].

TRACG has a multi-dimensional, two-fluid model for the reactor thermal hydraulics and a three-dimensional reactor kinetics model. The models can be used to accurately simulate a large variety of test and reactor configurations. These features allow for realistic simulation of a wide range of BWR phenomena, and are described in detail in the TRACG Model Description Licensing Topical Report [1].

TRACG has been extensively qualified against separate effects tests, component performance data, integral system effects tests and operating BWR plant data. The details are presented in the TRACG Qualification Licensing Topical Report [2]. Specific qualification studies for tests simulating passive BWR design features are reported in References 6 and 7.

1.2 PURPOSE AND SCOPE

The TRACG computer code is used to perform licensing analysis of the ESBWR. This report presents the methodology for application of TRACG to the ESBWR for stability analysis.

TRACG is specifically used for the following categories of analyses:

- Stability margins during normal operation including anticipated transients.

TRACG is also used to analyze plant startup trajectories, to assure a smooth ascension in pressure and power with a minimum of flow oscillation. Stability during plant startup is not a licensing issue; however, large MCPR margins are demonstrated for the startup scenario in this report.

This report describes the methodology to calculate key safety parameters and to quantify the uncertainties when applying the TRACG code to the ESBWR for the evaluation of stability margins. Thus, this report presents TRACG application methodology for ESBWR stability analysis. This document demonstrates the acceptable use of TRACG analysis results for licensing the ESBWR power plant within the applicable licensing bases.

The stability analysis will statistically account for the uncertainties and biases in the models and plant parameters using a Monte Carlo method for the Normal Distribution One-Sided Upper Tolerance Limit (ND-OSUTL) if the output distribution is normal, or the Order Statistics method if it is not (Section 7). Conservative values may be used in place of probability distributions for some plant parameters for convenience. The uncertainties and biases considered include the following:

- Model uncertainties
- Experimental uncertainties and any uncertainties related to test scale-up
- Plant uncertainties
- Process measurement errors
- Manufacturing tolerances

Some of these uncertainties are fuel type dependent. Therefore, periodic changes in the statistical analysis may be required as the core design changes. The statistical analysis process is defined in this report and criteria to be used to change this analysis are provided.

Representative results are shown that illustrate the application methodology and demonstrate the margins to the design limits. The overall analysis approach followed is consistent with the Code Scaling Applicability and Uncertainty (CSAU) analysis methodology [8]. Conformance with the CSAU methodology is demonstrated in Section 2. The sensitivity of the figure of merit (decay ratio) to the initial conditions is established in this report.

Section 2.0 describes the licensing requirements and the scope of the TRACG application to ESBWR stability. Section 3.0 describes the identification and ranking of phenomena relevant to stability. Section 4.0 describes and justifies the applicability of TRACG models for stability analysis. Section 5.0 describes the model uncertainties. Section 6.0 describes the application uncertainties and biases. Section 7.0 describes the method used for the combination of uncertainties. Section 8.0 provides a demonstration analysis and typical results. A discussion of plant startup in natural circulation is provided in Section 9.0.

1.3 SCOPE OF REVIEW

GE requests that the NRC approve TRACG for analyzing and demonstrating compliance with licensing limits for stability evaluation of the ESBWR.

The Licensing Topical Reports: TRACG Model Description [1]; TRACG Qualification; [2], TRACG Qualification for SBWR Volumes 1 and 2 [6], and TRACG Qualification for ESBWR [7] are incorporated by reference as part of the review scope.

2.0 LICENSING REQUIREMENTS AND SCOPE OF APPLICATION

2.1 LICENSING COMPLIANCE

The licensing basis for stability must comply with the requirements of 10 CFR 50, Appendix A, "General Design Criteria for Nuclear Power Plants". The Appendix A criteria related to stability are Criteria 10 and 12.

Criterion 10 (Reactor Design) requires that:

> "The reactor core and associated coolant, control, and protection systems shall be designed with appropriate margin to assure that specified acceptable fuel design limits are not exceeded during any condition of normal operation, including the effects of anticipated operational occurrences."

Criterion 12 (Suppression of Reactor Power Oscillations) requires that:

> "The reactor core and associated coolant, control, and protection systems shall be designed to assure that power oscillations which can result in conditions exceeding specified acceptable fuel design limits are not possible or can be reliably and readily detected and suppressed."

The ESBWR licensing basis for stability satisfies GDC 12 by designing the reactor system such that significant power oscillations are not possible. A high degree of confidence is established that oscillations will not occur by imposing conservative design criteria on the channel[1], core wide and regional decay ratios under all conditions of normal operation and anticipated transients.

Because oscillations in power and flow are precluded by design, the requirements of GDC 10 are met through the analysis for AOOs, and are automatically satisfied with respect to stability.

As a backup, the ESBWR will implement a Detect and Suppress solution as a defense-in-depth system. The details of the solution will be developed during the ESBWR Construction and Operating License (COL) phase.

2.2 STABILITY DESIGN CRITERIA

Compliance with General Design Criterion 12 is assured by implementing design criteria for the decay ratio. GE uses a stability criteria map of core decay ratio vs. channel decay ratio to establish margins to stability (Figure 2.2-1). Stability acceptance criteria for BWRs are established on this map at core decay ratio = 0.8 and limiting channel decay ratio = 0.8, with an allowance for regional mode oscillations in the top right corner of the defined rectangle. These boundaries were established considering model uncertainties of the order of 0.2 in the core and channel decay ratio in the GE analysis methods (FABLE and ODYSY). There is also margin in the regional boundary, which is drawn below available plant regional oscillation data, though the

[1] "Channel" is used interchangeably with "Bundle" in this report and denotes a fuel bundle and its channel box.

amount of conservatism has not been quantified. These criteria have been approved by the NRC for application of ODYSY to the E1A Long Term Stability Solution [12], [13].

The ESBWR stability design criteria are shown in this map in Figure 2.2-2. The ESBWR core size of 1132 bundles is significantly larger than the largest operating BWR (ABWR with 872 bundles). The sub-criticality of the azimuthal harmonic, which is relevant for regional oscillations, decreases with core size. The regional stability boundary is expected to move inwards in the Core Decay ratio vs. Channel Decay Ratio plane as the sub-criticality decreases. Figure 2.2-2 shows the approximate effect of the larger core size on the calculated regional stability boundary. The calculated values of higher harmonic sub-criticality for the ESBWR core vary between $0.76 and $0.95 (Section 8.1). These values are bounded by the estimated boundary for a sub-criticality of $0.70. In order to account for regional stability for the ESBWR, the acceptance criteria for the limiting channel decay ratio is constrained to be less than 0.5. This conservatively adjusts the operating plant criteria for the larger ESBWR core.

The design goal is for the nominal values of the core and channel decay ratios at rated power and flow to be less than 0.4 and 0.3 respectively, or about half the BWR acceptance criteria (where the channel decay ratio was reduced to approximately 0.6 to accommodate the regional stability boundary). Figure 2.2-2 shows that the design goal maintains a large margin to the onset of instability even with the reduction of the stable region on the stability map to account for the larger core size.

The design requirement is for the core and channel decay ratios to be less than the acceptance criteria of 0.8 and 0.5 at the 2σ level of uncertainty. Because the ESBWR is a new plant and there are no plant data, the uncertainties will include operating state and model uncertainties, even though there is already an explicit allowance for model uncertainty in the acceptance criteria.

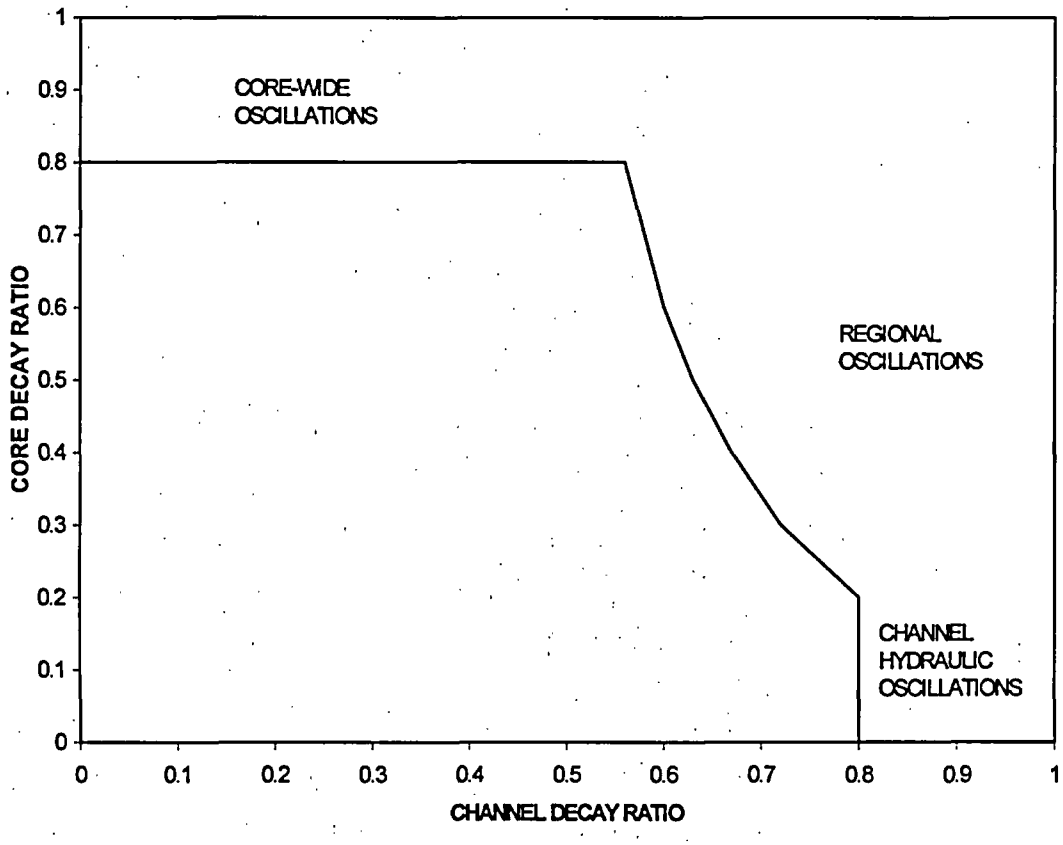

Figure 2.2-1: Stability Acceptance Criteria for BWRs

[[

]]

Figure 2.2-2: Proposed Stability Map for ESBWR

2.3 TRACG ANALYSIS APPROACH FOR LICENSING COMPLIANCE

The overall TRACG demonstration analysis approach for ESBWR stability analysis is consistent with the Code Scaling, Applicability and Uncertainty (CSAU) analysis methodology [8], and addresses the applicable elements of the NRC-developed CSAU evaluation methodology as described in the next section.

2.3.1 CONFORMANCE WITH CSAU METHODOLOGY

The CSAU report describes a rigorous process for evaluating the total model and plant parameter uncertainty for a nuclear power plant calculation. Further details on the CSAU methodology are contained in the NRC-issued Regulatory Guide 1.157 [9]. The CSAU methodology incorporates the elements of phenomena identification and ranking, documentation of models, assessment against Separate Effects Tests (SETs) and Integral System Tests (ISTs) for the key phenomena, and quantification of uncertainties due to the models, scaling and plant parameters. In the CSAU process, the overall model uncertainty is derived from the propagation of individual model uncertainties through code calculations; experimental comparisons are used as a check on the derived uncertainty.

The CSAU methodology consists of 14 steps, as outlined in Table 2.3-1.

The 14 CSAU steps are summarized in the following paragraphs. The objectives for each step are evaluated by indicating how they will be addressed in this report.

[1]. Specify scenario.

Stability analysis is performed at the limiting operating conditions including power, flow and exposure. Anticipated Operational Occurrences (AOOs) that might lead to more severe initial conditions for stability are also considered.

[2]. Select nuclear plant.

The Nuclear Power Plant (NPP) which is the basis for this application report is the 4500 MWt ESBWR, an optimized version of the plant described in the ESBWR Design Description [10].

[3]. Identify and rank phenomena.

All processes and phenomena that occur during an event do not equally influence plant behavior. The most cost efficient, yet sufficient, analysis reduces all candidate phenomena to a manageable set by identifying and ranking the phenomena with respect to their influence on the primary safety criteria. The processes and phenomena associated with each component are examined. After the processes and phenomena have been identified, they are ranked with respect to their effect on the primary safety criteria for the event. A phenomena identification and ranking table (PIRT) is established to guide the subsequent uncertainty quantification. The PIRTs for stability are reported in Section 3.

[4]. Select frozen code.

TRACG04 is the frozen code selected for the analysis.

[5]. Document code.

The details of the models are contained in the TRACG Model Description LTR [1]. A summary description of the TRACG assessment is provided in Section 2.3.2. Details are contained in the TRACG Qualification LTRs [2], [6], [7]. This report describes the application process. The User' Manual [11] provides guidance on the use of the code.

[6]. Determine code applicability.

To demonstrate applicability, one must begin with capability. Capability to calculate an event for a nuclear power plant rests on four elements: (1) conservation equations, which provide the code capability to address global processes; (2) constitutive correlations and models, which provide code capability to model and scale particular processes; (3) numerics, which provide code capability to perform efficient and reliable calculations; and (4) structure and nodalization, which address code capability to model plant geometry and perform efficient and accurate plant calculations. All four elements must be considered when evaluating the code capability for a specific application. Code capability is only one aspect needed to demonstrate that the code is applicable. Applicability also implies that the capability of the code has been demonstrated by actually applying the code in the intended manner with acceptable results. The capability of TRACG to model phenomena that are important to ESBWR simulations has been addressed in Section 4.1. Qualification aspects are addressed in Section 4.2.

[7]. Establish assessment matrix.

The determination of uncertainty for a computer code must be based on a sufficient data set, which necessarily will include both separate and integral effects tests and available plant data. The assessment matrix must cover all phenomena and components that were identified and ranked 'High' in the PIRT for the selected events for the nuclear power plant. The stability PIRTs are documented in Section 3.0. The assessment coverage of the PIRTs is summarized in Table 4.2-2.

[8]. Define nodalization for plant calculations.

The plant model must be nodalized finely enough to represent both the important phenomena and design characteristics of the nuclear power plant but coarsely enough to remain economical. In principle, nodalization can be treated as an individual contributor to code uncertainty; however, quantification of nodalization uncertainty can be very costly. Thus, the preferred path is to establish a standard nodalization based on the assessment against separate and integral effects tests. Nodalization studies have been performed in assessing this test data in order to determine the level of detail necessary to represent the important phenomena and then consistent levels of detail have been applied to establish standard noding schemes for the ESBWR. The standard ESBWR

nodalization for TRACG for stability applications is defined based on the qualification studies and is described in Section 5.

[9]. Determine code and experiment uncertainty.

Comparisons with separate effects tests are used to quantify the uncertainty in the individual models and correlations. Typically, experimental uncertainty is inherent in these comparisons and is not separated out. Quantification of the uncertainties in the model parameters is discussed in Section 5. The impact on the primary safety parameters for the nuclear power plant can be determined by varying the inputs to the individual models by a specified amount (e.g. $\pm$ 1σ). The overall uncertainty of the code in simulating the important phenomena for ESBWR stability is addressed fully in Section 8.

[10]. Determine effects of scale.

The differences for similar physical processes, at scales up to and including full scale, should be evaluated to establish a statement of potential scaling effects. For TRACG, this has been done by evaluating the experimental basis for the individual models and correlations against full-scale plant conditions, by performing qualification against separate-effects tests, integral effects tests at different scales and full-scale plant data, and by using a plant nodalization based on the qualification studies. Specific evaluations for stability are addressed in Section 5.

[11]. Determine effects of plant operating conditions.

Uncertainties in the nuclear power plant simulations may result from uncertainties in plant operating state or in plant process parameters. For example, the plant power distribution is a function of burnup history and control rod pattern prior to the transient. For the ESBWR, these uncertainties are accounted for by using the cycle exposure that leads to the highest decay ratios (Section 6). Uncertainties in setpoints will be treated by using analytical limits for these parameters.

[12]. Perform plant sensitivity calculations.

Nuclear power plant calculations for a given event are used to determine the code's output sensitivity (in the primary safety criteria parameters) to various plant operating conditions that arise from uncertainties in the reactor state at the initiation of the transient event or in plant process parameters. Similarly, nuclear power plant calculations are used to address the uncertainties introduced by the code models and correlations. In this manner, the sensitivities of the safety-related quantities to these parameters are evaluated individually or collectively. The sensitivity studies for stability are documented in Section 8.

[13]. Combine biases and uncertainties.

In this step, all the biases and uncertainties are combined into an overall bias and uncertainty. There are different techniques that can be used, as discussed in Section 7. The results of the stability analysis are shown in Section 8.

[14]. Determine total uncertainty.

The statement of total uncertainty for the code for ESBWR stability analysis is given in terms of the difference between the bounding and nominal results.

Table 2.3-1:

Code Scaling, Applicability and Uncertainty Evaluation Methodology

CSAU Step	Description	Addressed In
1	Scenario Specification	Normal operation, AOOs, plant startup
2	Nuclear Power Plant Selection	ESBWR 4500 MWt
3	Phenomena Identification and Ranking	Table 3.1-1
4	Frozen Code Version Selection	TRACG04
5	Code Documentation	References [1,2,6,7,11]
6	Determination of Code Applicability	Table 4.2-1
7	Establishment of Assessment Matrix	Table 4.2-2
8	Nuclear Power Plant Nodalization Definition	Section 5
9	Definition of Code and Experimental Accuracy	Section 5
10	Determination of Effect of Scale	Section 5
11	Determination of the Effect of Reactor Input Parameters and State	Section 6
12	Performance of Nuclear Power Plant Sensitivity Calculations	Section 8
13	Determination of Combined Bias and Uncertainty	Section 8
14	Determination of Total Uncertainty	Section 8

2.4 IMPLEMENTATION REQUIREMENTS

The implementation of TRACG into actual licensing analysis of ESBWR stability is contingent upon completion of the following implementation requirements:

- Review and approval by the NRC of:
  1. The uncertainties documented in Section 5.
  2. The statistical process for analyzing stability margins described in Section 7.
- Calculation of overall biases and uncertainties to be applied to best-estimate calculations of decay ratios as shown in Section 8.

2.4.1 REVIEW REQUIREMENTS FOR UPDATES

In order to effectively manage the future viability of TRACG for ESBWR stability licensing calculations, GE proposes the following requirements for upgrades to the code to define changes that (1) require NRC review and approval and (2) that will be on a notification basis only.

2.4.1.1 UPDATES TO TRACG CODE

Modifications to the basic models described in Reference 1 may <u>not</u> be made for ESBWR stability licensing calculations without NRC review and approval.

Features that support effective code input/output may be added without NRC review and approval.

2.4.1.2 UPDATES TO TRACG MODEL UNCERTAINTIES

New data may become available with which the specific model uncertainties described in Section 5 may be reassessed. If the reassessment results in a need to change specific model uncertainty, the specific model uncertainty may be revised for ESBWR stability licensing calculations without NRC review and approval as long as the process for determining the uncertainty is unchanged.

2.4.1.3 UPDATES TO TRACG APPLICATION METHOD

Revisions to the TRACG application method described in Section 7 may <u>not</u> be made for ESBWR stability licensing calculations without NRC review and approval.

2.4.1.4 CYCLE SPECIFIC UNCERTAINTIES IN SAFETY PARAMETERS

Biases and uncertainties in the decay ratios are developed for the ESBWR plant using the process described in this report. This process will be implemented for the first operating cycle for the ESBWR. The magnitudes of these biases and uncertainties may change for future core designs and do not require NRC review and approval. The values of the uncertainties will be transmitted to the NRC for information if the stability margin is significantly impacted.

2.5 RANGE OF APPLICATION

The intended application is ESBWR stability analysis at normal operation including potentially more severe conditions resulting from AOOs.

3.0 PHENOMENA IDENTIFICATION AND RANKING

The critical safety parameter for evaluating stability margin is the decay ratio. The phenomena identification and ranking table (PIRT) is used to delineate the important physical phenomena that impact the decay ratio. PIRTs are ranked with respect to their impact on the critical safety parameters. For example, the decay ratio is determined by the reactor response to perturbations in core flow or system pressure. The coupled core neutronic and thermal-hydraulic response to void propagation through the core is determined by the void reactivity, fuel rod thermal inertia and core pressure distribution.

3.1 ESBWR STABILITY PIRT

All processes and phenomena that occur during a transient do not equally influence plant behavior. Disposition analysis is used to reduce all candidate phenomena to a manageable set by identifying and ranking the phenomena with respect to their influence on the critical safety parameters. The processes and phenomena associated with each component are examined, and then ranked with respect to their effect on the critical safety parameters for the event.

PIRTs are developed with only the importance of the phenomena in mind and are independent of whether or not the model is capable of handling the phenomena and whether or not the model shows a strong sensitivity to the phenomena. For example, two phenomena may be of high importance yet may tend to balance each other so that there is little sensitivity to either phenomenon. Both phenomena are of high importance because the overall balance between these competing phenomena is important.

Table 3.1-1 was originally developed to identify the phenomena that govern BWR/3-6 stability responses, and represents a consensus of GE expert opinions. The phenomena were then reviewed for the ESBWR and some changes were incorporated. The differences between the operating plants and the ESBWR have been identified in the table. The stability transient events have been categorized into three distinct groups:

- Channel thermal-hydraulic instability,
- Core-wide instability, and
- Regional instability.

For each event type, the phenomena are listed and ranked for each major component in the reactor system. The ranking of the phenomena is done on a scale of high importance to low importance or not applicable, as defined by the following categories:

- **High importance (H):** These phenomena have a significant impact on the decay ratio and should be included in the overall uncertainty evaluation.
- **Medium importance (M):** These phenomena have minor impact on the decay ratio and may be excluded in the overall uncertainty evaluation.
- **Low importance (L) or not applicable (NA):** These phenomena have no impact on the decay ratio and need not be considered in the overall uncertainty evaluation.

In the PIRT (Table 3.1-1), the High and Medium ranked phenomena are highlighted in red. Differences between the ESBWR PIRT and that for the operating BWRs (regardless of ranking) are marked in green.

The parameters that are important for stability are those that determine the natural circulation flow, density wave propagation in the core and the feedbacks to the density wave propagation. The natural circulation flow is governed by the resistance and density distribution in the flow loop. The important resistances in the flow loop are in the core, separators and to a smaller extent, the lower plenum. The density distribution depends on the void fractions in the chimney, core, and separators. Density wave propagation and phase lags are dependent on the core velocities and void distribution as well as the core pressure drop distribution. Feedbacks include those between the core density and neutron flux, and between the neutron flux and fuel rod heat flux. For the regional mode of oscillation, the sub-criticality of the higher order harmonics of the neutron flux distribution is an important parameter.

Differences between the ESBWR PIRT and the corresponding table for operating plants result from two sources:

1. Differences in geometrical configuration

   The ESBWR incorporates a tall chimney region to enhance natural circulation (Figure 3.1-1). The partitioned chimney introduces a number of new phenomena to be considered. Each chimney cell receives the flow from a group of 16 bundles together with the core bypass region between these 16 bundles (Figure 3.1-2). The chimney cells communicate with each other at the top of the chimney (6 m above the top of the core) and also through the top guide at the top of the bypass region. Because the 16 bundles feeding a chimney are coupled to a common chimney cell, the stability of this group of bundles (dubbed a "super bundle") is also evaluated. Chimney cells in the peripheral region of the core have a lower void fraction and higher density than those in the central region. Thus, the pressure at the bottom of a peripheral chimney cell is higher than for a central chimney cell. The pressure difference can result in a small flow down from a peripheral cell through the top guide and into the central chimney cells. The axial resistance of the top guide and the radial resistance across the bypass region play a role in determining the magnitude of this recirculation flow and possible ingestion of steam into the top of the bypass region.

2. Different figure of merit

   Because sustained oscillations are precluded in the ESBWR, the figure of merit is the decay ratio. Phenomena related to CPR or core heatup are not important for the ESBWR and have been relegated to the "Low" importance category.

For the core region, Table 3.1-1 also tabulates a number of derived parameters (e.g. ratio of core power to core flow) important to reactor stability. While these can be obtained as ratios of parameters defined earlier in the table, in many cases the ratios are better indicators of stability margins than the individual parameters.

Table 3.1-2 evaluates initial conditions and plant parameters for their importance to stability. These are not physical phenomena but determine the plant state, and have been kept separate from the phenomena in Table 3.1-1.

The PIRT serves a number of purposes. First, the phenomena are identified and compared to the modeling capability of the code to assess whether the code has the necessary models to simulate the phenomena. Second, the identified phenomena are cross-referenced to the qualification basis to determine what qualification data are available to assess and qualify the code models and to determine whether additional qualification is needed. Third, the High-ranked parameters are varied over their uncertainty distributions to obtain an overall uncertainty in the estimate of the safety parameters.

Table 3.1-1:
Phenomena Governing ESBWR Stability Transients

[[

]]

Table 3.1-2:
Initial Conditions and Plant Parameters

[[

]]

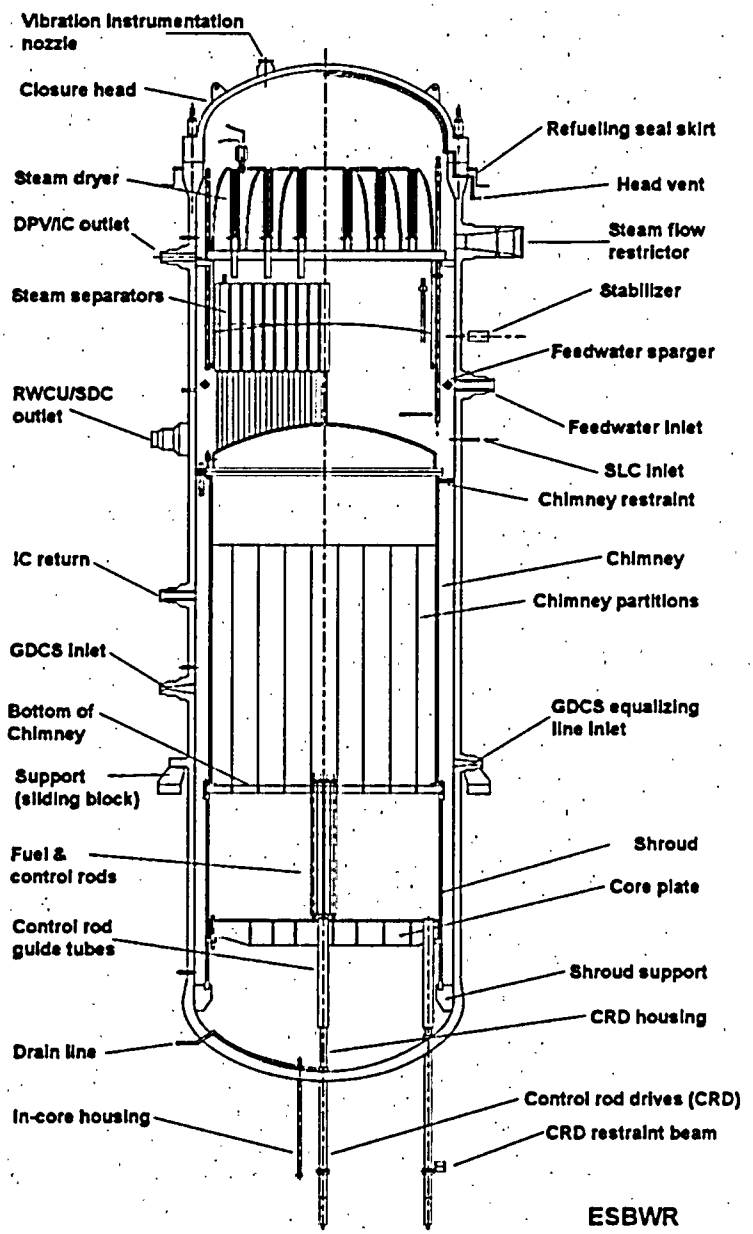

Figure 3.1-1: Schematic of ESBWR Vessel and Internals

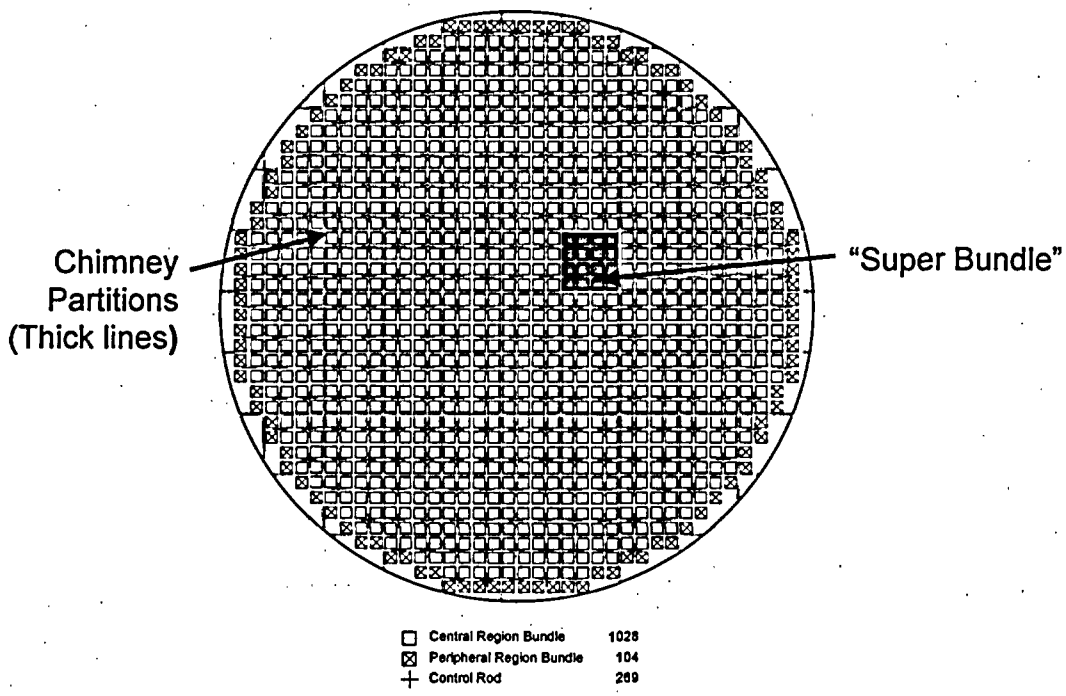

Figure 3.1-2: Top View of ESBWR Chimney and Core Region

4.0 APPLICABILITY OF TRACG TO ESBWR STABILITY ANALYSIS

This section demonstrates the applicability of TRACG for the analysis of stability for ESBWR through a two-step process. First, the phenomena identified in Section 3 are compared to the modeling capability of the code to determine that the code has the necessary models to simulate the phenomena. Second, the assessment basis of the TRACG code for stability applications is examined.

4.1 MODEL APPLICABILITY

The capability of the code to simulate an event for a nuclear power plant depends on four elements:

- Conservation equations, which provide the code capability to address global processes,
- Correlations and models, which provide the code capability to model and scale particular processes,
- Numerics, which provide the code capability to perform efficient and accurate calculations, and
- Structure and nodalization, which address the code capability to model plant geometry and perform efficient and accurate calculations.

Consequently, these four elements must be considered when evaluating the applicability of the code to the event of interest for the nuclear power plant calculation. The key phenomena for stability analysis were identified in the PIRTs in the previous section. The capability of the code to simulate the key phenomena is addressed, documented and supported by code qualification in References 1,2,5,6 and 7. The results are summarized in this section.

The complete list of phenomena is cross-referenced to the model capabilities in Table 4.2-1. The table shows that TRACG has models to treat the relevant phenomena for stability analysis.

4.2 ASSESSMENT MATRIX

The identified phenomena are cross-referenced to the qualification basis to determine what qualification data are available to assess and qualify the code models, and to determine whether additional qualification is needed for some phenomena.

The qualification assessment of TRACG models is summarized in Table 4.2-2. For each PIRT phenomenon that is ranked High or Medium, the relevant elements from the Qualification LTR [2] are identified. The table shows that for almost all the governing stability-related phenomena, TRACG qualification has been performed against a wide range of data. Data from separate-effects tests, component tests, integral system tests and plant tests as well as operating plant data have been used to qualify the capability of TRACG to model the phenomena.

The exceptions where there is no data coverage are: lower plenum radial flow resistance; core bypass region axial and radial flow resistance; and chimney cell interactions. The flow resistances are based on handbook correlations. Large uncertainties will be applied to these parameters in the statistical process of calculating upper bounds for the decay ratio. There is no

direct data for chimney cell interactions, but there are no new phenomena to be considered. The response of individual channels, which are part of a 16-bundle cluster under a chimney cell, is analyzed in detail as part of channel stability evaluations.

A large part of the assessment basis (particularly for neutronics related phenomena) consists of plant stability data. These data are primarily for onset of oscillations; i.e., at decay ratios close to 1. It was judged necessary to expand this data base to include plant data at low decay ratios, typical of ESBWR operation. For this purpose, additional TRACG assessment results versus Peach Bottom stability data with low decay ratio are included later in this section.

Table 4.2-1

Stability Phenomena and TRACG Model Capability Matrix

[[

]]

Table 4.2-2:

Qualification Assessment Matrix for High and Medium Ranked ESBWR Stability Phenomena

[[

]]

4.3 OTHER TOPICS RELEVANT TO TRACG MODELING OF INSTABILITY

This section addresses other topics relevant to TRACG modeling of instability, including the selection of numerical integration scheme and numerical formulations used for stability analysis.

4.3.1 EXPLICIT INTEGRATION SCHEME FOR THE CHANNEL COMPONENT

TRACG uses a fully implicit integration technique for the heat conduction and hydraulic equations when integrating from time step n to time step n+1. In the implicit formulation, the convective terms are calculated based on the new properties at time step n+1. The fully implicit technique is the default option. The governing hydraulic equations in the implicit form are provided in Section 8.2 of Reference 1. For time domain stability calculations, an optional explicit integration technique is employed for the channel component. To minimize numerical damping, the use of the explicit scheme changes the convective terms to use the current properties at time step n in place of the new properties at time step n+1.

The TRACG thermal-hydraulic instability modeling using the explicit integration scheme has been evaluated for adequacy by comparison to experimental data from the FRIGG facility, as discussed in Section 3.7 of Reference 2. Two types of tests were run in the FRIGG facility. One test series used a pseudo random signal imposed on the system to determine the system response as a function of frequency. A second test series provided a more deterministic measurement of the onset of unstable behavior. In these tests, which started from steady-state natural circulation operation, the system power was slowly increased until the onset of unsteady behavior was observed. This second series of tests have been simulated by TRACG. Comparisons of TRACG predictions of the channel power for the onset of limit cycle oscillations to the power measured in the tests is considered the best assessment of the code's ability to predict the onset of unstable operation.

4.3.2 COUPLING OF CONDUCTION AND HYDRAULIC EQUATIONS

The coupling scheme used for the conduction and hydraulic equations does not change for stability applications, relative to AOOs.

The heat transfer coupling between the structures and the hydraulics is treated implicitly, when the implicit integration technique is used. For this purpose, the heat conduction equation is solved in two steps, and thus integration of the combined equations involves the following steps:

(1) The heat conduction equation for structures is linearized with respect to fluid temperatures. The result of this step is a system of linear equations for structure temperatures and surface heat flow as functions of the fluid temperatures.

(2) The hydraulic equations are solved using an iterative technique. This step results in new values for the fluid pressures, void fraction, temperatures and velocities.

(3) A corrector step is utilized for the hydraulic solution. Due to the use of an iterative solution technique, the conservation of the properties is affected by the convergence. The corrector step is employed to correct any lack of conservation due to imperfect convergence.

(4) Back-substitution into the heat conduction equation is performed to obtain new temperatures for structures.

The linearization of the heat conduction equation and subsequent back-substitution (Steps 1 and 4) are described in Section 8.1 of Reference 1. The hydraulic solution (Steps 2 and 3) is described in Section 8.2 of Reference 1.

4.3.3 COUPLING OF THE VESSEL AND CHANNEL COMPONENTS

The coupling scheme used between the vessel component and the channel components does not change for stability applications, relative to AOOs. A network solution scheme is applied, as described in Section 8.2.2 of Reference 1. For stability calculations, the numerical method is selected on a component-by-component basis. Explicit integration is used for the channel component and the other components use the implicit numerical method. When a component using an implicit numerical method is connected to a component using the explicit numerical method, the new time step fluid properties are convected between the two components. Thus the component using the implicit numerical method is fully implicit for all nodes. The explicit component is fully explicit for all nodes except for a node connecting to an implicit component, which will use a mixture of old time step and new time step properties in the convective terms. Old time step properties are used in the convection to other cells in the explicit component and new time properties are used in the convection at a face connecting to an implicit component. With this approach conservation of mass and energy balances is assured.

4.3.4 COUPLED 3-D KINETICS AND THERMAL-HYDRAULICS MODEL

The coupled 3-D kinetics and thermal-hydraulics model used does not change for stability applications, relative to AOOs. The 3-D kinetics model is described in Section 9 of Reference 1.

TRACG solves the three-dimensional (3-D) transient neutron diffusion equations using one neutron energy group and up to six delayed neutron precursor groups. The basic formulation and assumptions are consistent with the GE 3-D BWR Core Simulator [14]. The neutron flux and delayed neutron precursor concentrations at every (i,j,k) node are integrated in time in response to moderator density, fuel temperature, boron concentration or control rod changes. [[

]]

[[

]]

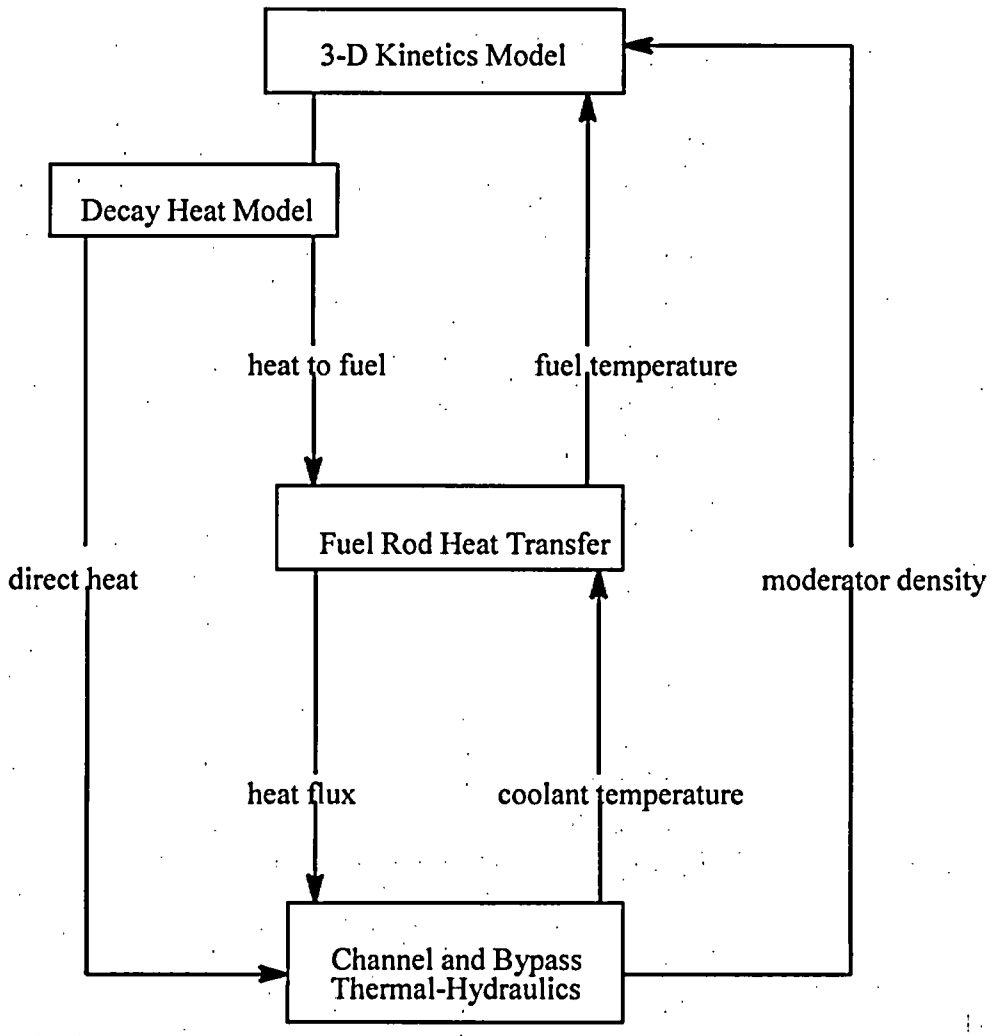

Figure 4.3-1: Data Transfer Between TRACG Models

4.4 TRACG QUALIFICATION AGAINST PEACH BOTTOM UNIT 2 STABILITY DATA

Low flow stability tests were conducted at Peach Bottom 2 at the end of Cycle 2 on April 14, 15 and 16, 1977 [23]. Chronologically, these tests were performed during the same period as the well-known turbine trip tests, in between Turbine Trip 1 (April 9) and Turbine Trip 2 (April 23). The stability tests (PT1 through PT4) were conducted along the low-flow end of the rated power-flow line, and along the power-flow line corresponding to minimum pump speed. The reactor core stability margin was determined from an empirical model fitted to the experimentally derived transfer function measurement between core pressure and the APRM (Average Power Range Monitor) neutron flux signal. Both periodic and pseudo-random binary signals were applied to the pressure regulator set point as the input signal.

The pseudo-random binary perturbation technique was found to be an operationally simple and precise technique for measuring BWR core stability margins. The tests demonstrated large stability margins (low decay ratios) for the Peach Bottom 2 Cycle 2 core design.

4.4.1 TEST CONDITIONS AND TEST RESULTS

The operating conditions at which the low flow stability tests were conducted are listed in Table 4.4-1. The minimum core flow that could be achieved at test conditions PT2, PT3 and PT4 was limited to about 20% of rated recirculation pump speed rather than natural circulation core flow, as originally planned. The test points are shown on the power-flow map in Figure 4.4-1. The process computer average axial power distributions for the four tests are shown in Figure 4.4-2. The experimentally obtained transfer function between APRM A and core pressure was fit to a second order function with one real zero and two complex poles. In the Laplace domain the transfer function is of the form:

$$G(s) = \frac{K_P(\tau_1 s + 1)}{s^2/\omega_1^2 + 2\delta_1 s/\omega_1 + 1}$$

where δ_1 is the damping ratio, ω_1 the natural frequency and K_p is the gain. The decay ratio is then calculated as:

$\ln DR = \frac{-2\pi\delta_1}{\sqrt{1-\delta_1^2}}$ Data for resonant frequency, damping ratio and decay ratio are presented in Table 4.4-2 for the four tests.

4.4.2 TRACG ANALYSIS

The TRACG input decks used for PB2 Turbine Trip Test 1 (TT1) were the starting point for the TRACG analysis. As the stability tests were conducted just a week following TT1, the exposure accounting data generated for TT1 were applicable for the stability tests. PANAC wrapups were created for the specific test by modifying the initial conditions (flow, power, pressure, core inlet enthalpy and control rod pattern. Figure 4.4-2 shows the average axial power shapes from the process computer for the four tests. The TRACG input deck used for TT1 was modified to nodalize the fuel channels more finely near the boiling boundary, as discussed in Section 5.2. The PB2 core, consisting of 7x7 and 8x8 fuel, was modeled with eight channel groups, as shown in Table 4.4-3.

Stability analysis was performed by perturbing the turbine inlet pressure. Various types of perturbations were tried. Results were insensitive to the method of perturbation (as shown later in this section). A pressure pulse of 0.06 MPa (10 psi) for 1 second has been used in the cases for which results are reported below.

Figure 4.4-3 shows the power response to a pressure pulse applied at the turbine inlet for Test PT1. A decay ratio and frequency of oscillation can be extracted from this trace. The decay ratio is not exactly constant for the non-linear system. In order to have a common basis for comparison, the decay ratio has been defined as the ratio of the amplitudes of the second negative peak to the first negative peak. The power responses to pressure perturbations for the test conditions PT2, PT3 and PT4 are shown in Figure 4.4-4 to Figure 4.4-6. Measured and calculated decay ratios and frequencies are compared in Table 4.4-4. Calculated decay ratios are also compared with data in Figure 4.4-1. Generally, TRACG is a little conservative in its predictions. For these four data points, the TRACG calculations have a mean error of [[ ]]and a standard deviation of [[ ]]. TRACG calculates a damped natural frequency of about [[ ]]Hz, considerably lower than the [[ ]] Hz measured in the tests. The frequencies calculated by TRACG correlate well with the transit time for the vapor through the high power channels. The reason for the higher frequencies seen in the data has not been identified, but may be due to the method of extracting them from the transfer function.

4.4.3 SENSITIVITY STUDIES

TRACG sensitivity studies were performed for Test PT1 to evaluate the effect of the nature of the perturbation applied to initiate the power response. The sensitivity studies and results are reported in Table 4.4-5. Rectangular pressure pulses of different amplitude were applied for different durations. A triangular pressure pulse was also applied in one case. Finally, two perturbations in core flow of different amplitude were tried. The results are insensitive to the magnitude, shape and duration of the pressure pulses. Only the smaller core flow perturbation led to a slightly larger decay ratio – largely due to a small amplitude power response (Figure 4.4-8). These results provide confidence in this technique of estimating decay ratios. Subsequently, the rectangular pressure pulse of 0.06 MPa for 1 s has been used for the other calculations.

The sensitivity to core nodalization, specifically channel grouping, was also evaluated for all four tests. The core was modeled with 19 channel groups, conventionally used for regional stability calculations with TRACG. The results (shown in Figure 4.4-9 for Test PT2) were virtually identical for the two cases. Thus, the 8-group nodalization is judged to be adequate for these calculations.

4.4.4 CHANNEL DECAY RATIO

There are no measurements of the channel decay ratio. TRACG calculations of channel decay ratio were made by perturbing the inlet flow to an individual channel, with the power kept constant. The resulting channel flow response for conditions corresponding to PT3 is shown in Figure 4.4-10. The channels are very stable, with decay ratios close to zero.

Table 4.4-1:

PB2 Operating Conditions for Stability Tests

Test Number	Reactor Power		Core Flow Rate		Core Pressure	Core Inlet Enthalpy
	MWt	% Rated	kg/s	% Rated	MPa	kJ/kg
PT1	1995	60.6	6629	51.3	6.895	1183
PT2	1702	51.7	5419	42.0	6.839	1174
PT3	1948	59.2	4903	38.0	6.929	1182
PT4	1434	43.5	4903	38.0	6.888	1179

Table 4.4-2:

PB2 Stability Test Results

Test Number	Closed Loop Resonant Frequency (Hz)	Damping Coefficient	Decay Ratio
PT1	0.44	0.318	0.12
PT2	0.47	0.319	0.12
PT3	0.44	0.168	0.34
PT4	0.40	0.190	0.30

Table 4.4-3:

TRACG Channel Grouping for PB2 Core

Channel Component #	Bundle Type	Channel Location	Number of Physical Channels	Channel Average Power (MW)
11	7X7	CENTRAL	68	2.77
14	8X8	CENTRAL	20	3.13
12	7X7	CENTRAL	240	2.64
15	7X7	CENTRAL	176	2.61
16	8X8	CENTRAL	60	2.96
17	8X8	CENTRAL	104	2.94
18	7X7	CENTRAL	4	3.11
13	7X7	PERIPHERAL	92	1.69

Table 4.4-4:
Comparison of TRACG Predictions with Test Data

[[

]]

Table 4.4-5:
Sensitivity to Applied Perturbations

[[

]]

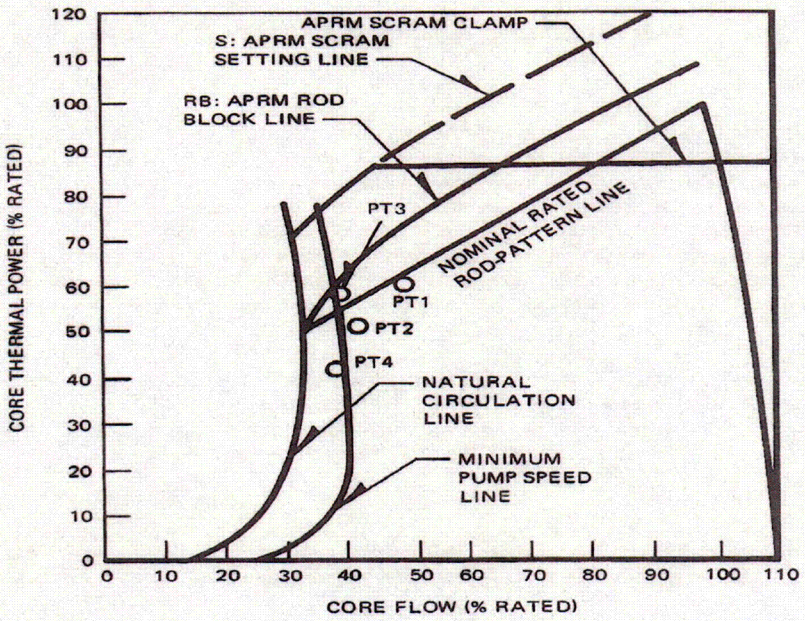

Figure 4.4-1: Test Conditions on PB2 Power/Flow Map

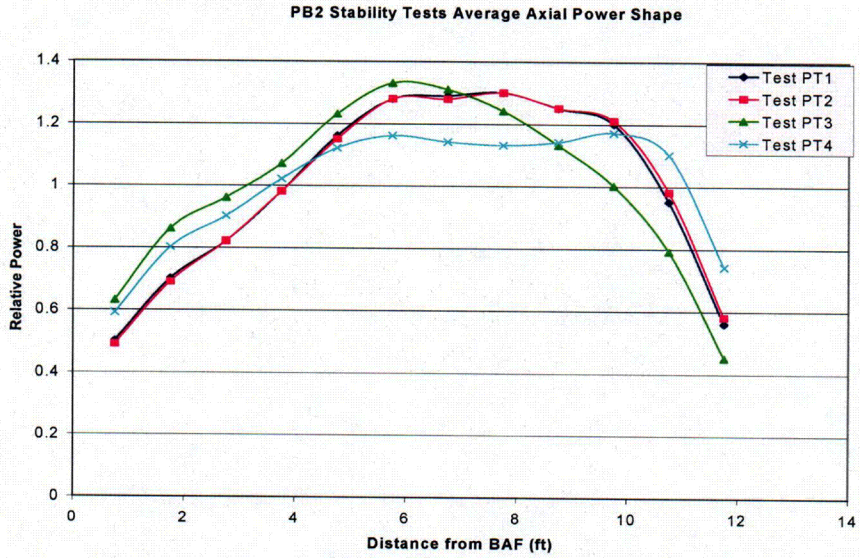

Figure 4.4-2: Average Axial Power Shapes for Stability Tests

C-01

[[

]]

Figure 4.4-3: Power Response to Pressure Perturbation for Test PT1

[[

]]

Figure 4.4-4: Power Response to Pressure Perturbation for Test PT2

[[

]]

Figure 4.4-5: Power Response to Pressure Perturbation for Test PT3

[[

]]

Figure 4.4-6: Power Response to Pressure Perturbation for Test PT4

[[

]]

Figure 4.4-7: TRACG Predictions of Decay Ratio versus Data

[[

]]

Figure 4.4-8: Sensitivity to Core Flow Perturbation Amplitude

[[

]]

Figure 4.4-9: Sensitivity to Number of Channel Groups (Test PT2)

[[

]]

Figure 4.4-10: Channel Decay Ratio for Test PT3

5.0 MODEL BIASES AND UNCERTAINTIES

The model biases and uncertainties for all items from the PIRT table (Table 3.1-1), which have been identified as having a significant impact on the decay ratios, have been evaluated. The subset of phenomena ranked High or Medium is included in the Qualification Assessment Matrix (Table 4.2-2). Overall model biases and uncertainties for the stability application are assessed for each high and medium ranked phenomenon by using a combination of comparisons of calculated results to: (1) separate-effects test facility data, (2) integral test facility test data, (3) component qualification test data and (4) BWR plant data. Where data are not available, cross-code comparisons or engineering judgment are used to obtain approximations for the biases and uncertainties. For some phenomena that have little impact on the calculated results, it is appropriate to simply use a nominal value or to conservatively estimate the bias and uncertainty. Table 5.1-4 provides the dispositions of the high and medium ranked stability model parameters from Table 4.2-2.

5.1 MODEL PARAMETERS AND UNCERTAINTIES

This section discusses the uncertainties associated with each item that has been identified as having an impact on the decay ratio for either channel, core wide or regional stability. The ID, description, and highest ranking (M for Medium and H for High) are listed for each item. The results are summarized in Table 5.1-4.

A11 Lower Plenum Radial Resistance, M

The lower plenum radial resistance is a contributor to the overall loop resistance that determines the natural circulation flow through the core. While this is a minor resistance compared to the core and separators, the uncertainty is fairly large because of the complex path through the guide tubes. [[

]]

B2 Bypass Void Distribution, M

The bypass void fraction is controlled by the vapor generation in the bypass and the relative velocity between the phases. Heat generation in the bypass region and wall heat transfer from the fuel bundles determine the vapor generation in the bypass region. Heat generation is due to direct moderator heating (B13). The uncertainty in the wall heat transfer is due to nucleate boiling heat transfer and is not a major contributor. The void fraction is determined by the relative velocity between the phases, which depends on the interfacial shear. The uncertainty in the interfacial shear is defined in Item C2AX. It is possible for voids to be drawn into the top of the bypass region from the chimney in the peripheral region. The magnitude of the void fraction due to this effect is governed by the axial and radial resistance at the top of the bypass (B14).

B13 Bypass Direct Moderator Heating, M

The direct moderator heating is the result of energy released into the moderator as the fast neutrons are slowed down and due to gamma absorption. The uncertainty is defined in Item C3DX.

B14 Bypass Axial and Radial Resistance, M

The chimney cells formed by the partitions in the chimney communicate at the bottom via the top of the core bypass region. The peripheral chimney cells are at a higher pressure at the bottom level with respect to the central chimney cells because of the higher static head in these cells. The pressure differential results in a small downflow at the top of the bypass in the peripheral cells and a crossflow to the central region of the bypass where the flow turns upwards and returns to the chimney. This circulation pattern can draw steam into the bypass from the chimney region. The extent to which voids exist at the top of the bypass depends on the relative magnitude of the bypass resistance to the flow resistance of the flow openings at the bottom of the chimney. [[

]].

C1AX Void Coefficient, H

TRACG04 uses a 3-D neutron kinetics model based on the PANACEA [14] neutronics parameters as they are implemented in PANAC11. The nodal reactivity is calculated in terms of the infinite multiplication factor, migration area, fast group removal cross-section and fast group diffusion coefficient. All of these parameters are calculated in terms of the moderator density. The infinite multiplication factor is also dependent on a history-weighted moderator density and nodal exposure.

[[

]]

[[

]]

Figure 5.1-1: TGBLA06 Void Coefficient Relative Bias and Relative Standard Deviation for Various Exposures (GWd/MT)

C1DX 3-D Kinetics and Power Shape, H

TRACG has a 3-D neutron kinetics model, based on the PANACEA formulation [14]. The TRACG kinetics model has been qualified against stability data for various BWRs, viz. LaSalle 2, Leibstadt. Steady-state power distribution comparisons have been made with data from several plants [2] and PANACEA predictions. The uncertainty of the kinetics model is determined by the uncertainty in scram reactivity, void and Doppler coefficient. For stability evaluations which involve the response to small perturbations, only the void reactivity is relevant.

C1EX Delayed Neutron Fraction, H

The delayed neutron fraction is important in determining the neutronic response speed. This parameter is a function of the fuel type and exposure. The variability in delayed neutron fraction is covered by considering the full range of fuel types and core exposures. Note that the dynamic void coefficient (obtained by dividing the void coefficient by the delayed neutron fraction) is a better parameter for stability evaluations than the void coefficient. Thus, observations related to the dynamic void coefficient in subsequent sections refer to both C1AX and C1EX. Similarly, the parameter CS4 (sub-criticality of the 1st harmonic) is conventionally represented in dollars by dividing the difference in eigenvalues for the fundamental and first harmonic modes by the delayed neutron fraction.

C1FX Sub-criticality of First Harmonic Mode, H

The sub-criticality of the first harmonic mode governs the likelihood of regional oscillations. The sub-criticality must be overcome by the gain of the hydraulic transfer function. Hence, the smaller the sub-criticality, the easier it is to excite the harmonic mode oscillations. This parameter is covered by considering the cycle exposure that produces the lowest sub-criticality.

C2AX Interfacial Shear, H

Although this PIRT phenomenon is entitled "Interfacial Shear", it more generally concerns representation of the uncertainties of TRACG model parameters that affect the prediction of void fraction in the core and bypass. The core and bypass are distinguished from the regions of the vessel discussed under E2 and F1 by their comparatively small hydraulic diameters. As described in the AOO application report [3], data from the FRIGG test facility [19], which form the basis for the GE design void correlation, are the most relevant data for pressures near the normal operating range. TRACG02 predictions of the FRIGG void fraction data for fully developed nucleate boiling showed a small positive bias in absolute void fraction of [[ ]] and a standard deviation of [[ ]] [3]. The uncertainty observed in these data comparisons was reflected in the TRACG02 model through a PIRT multiplier (PIRT22) on the interfacial shear parameter (C_o-1). The relatively small bias in the predictions, especially in comparison with the experimental uncertainty of [[ ]] in the void fraction measurement, was used to justify the choice of an unbiased mean of [[ ]] for PIRT22. From an examination of the dependence of void fraction predictions on PIRT22, it was concluded that a PIRT22 standard deviation of [[ ]] would appropriately represent the prediction standard deviation of [[ ]]. (As described in the AOO application report [3], the error in the TRACG

predictions is somewhat larger for subcooled boiling. This is attributed to uncertainty in the onset of net vapor generation, which is covered under C2BX.)

The predictions of the FRIGG data were repeated with TRACG04. The results gave a bias of [[ ]] and a standard deviation of [[ ]], differing only slightly from the results obtained using TRACG02. Thus, the uncertainty (standard deviation of [[ ]]) in PIRT22 has been retained.

C2BX Subcooled Boiling, H

For stability evaluations, interfacial heat transfer is a factor only in the subcooled boiling region. The void fraction in the subcooled flow regime is quite insensitive to the magnitude of the heat transfer coefficients at the interface between the bubbles and the subcooled liquid, as long as a reasonable value is used. The void fraction is more sensitive to the liquid enthalpy at which net vapor generation occurs (h_{ld}), and to the distribution of the surface heat flux going into vapor generation versus liquid superheat at the wall (q''_l). The Saha-Zuber criterion is used for h_{ld} and the Rouhani-Bowring model is used to calculate the fraction of the wall heat flux to the liquid, q''_l [1]. Of these, the void fraction is most affected by h_{ld}. Reference 20 shows that the scatter in the prediction of the subcooling at the net vapor generation point, $h_f - h_{ld}$, can be bounded by ± [[ ]]. Comparisons to 8x8 bundle void fraction data show that the larger scatter in the void fraction for low qualities in the subcooled boiling region ([[ ]] for the fully developed nucleate boiling region) is covered when a [[ ]] perturbation is applied to the subcooling for the onset of net vapor generation. The mean error is also slightly larger for subcooled boiling ([[ ]]). The statistical analysis of the comparison to the subcooled void fraction data is shown in Figure 5.1-2.

A [[ ]] variation in the subcooling for onset of net vapor generation corresponds to an average of [[ ]] and a maximum of [[ ]] variation in the void fraction for the subcooled boiling region. Therefore a 1σ uncertainty of [[ ]] is assigned for this model. The impact on the calculated void fraction at the FRIGG test conditions of a PIRT multiplier (PIRT23) value of [[ ]] is seen in Figure 5.1-3.

[[

]]

Figure 5.1-2. FRIGG OF64 Void Fraction Data – Subcooled Boiling

[[

]]

Figure 5.1-3. Void Fraction Sensitivity to PIRT23

C3AX Pellet Heat Distribution, H

The pellet power distribution is calculated by lattice physics codes and provided as an input to TRACG. Uncertainties in this parameter are reflected in the pellet temperature distribution, which is the parameter for which data are available. [[

]] Sensitivity studies show that the distribution calculated by lattice physics codes provides conservative results compared to a flat power distribution.

C3BX Pellet Heat Transfer Parameters, H

The TRACG fuel rod model is based on the GESTR model [21]. The uncertainty in measured fuel centerline to coolant temperature differences is [[ ]] and includes uncertainty in gap size and conductance, pellet conductivity and power distribution. The uncertainties in pellet power distribution, pellet conductivity and gap conductance are lumped into a single uncertainty in the fuel conductivity, in qualifying the overall model against fuel temperature data. The dominant resistance is the pellet conductivity; an [[ ]] variation in the pellet conductivity corresponds to the [[ ]] observed uncertainty in the centerline to coolant difference, while the gap conductance needs to be varied by a factor of [[ ]] to produce the same variation in the temperature difference as shown in Figure 5.1-4 and Figure 5.1-5. In these figures, PIRT27 is a multiplier on the fuel thermal conductivity and PIRT28 is the multiplier on the gap conductance. When the gap conductance is increased, the resistance over the gap becomes insignificant compared to the thermal resistance of the pellet, and it is not possible to vary the temperature difference to the 2σ level needed to produce a 95% probability estimate. Furthermore, normal distribution in the gap conductance would not produce a normal distribution in the center to fluid temperature difference due to the highly non-linear relationship between the gap conductance and the fuel center to fluid temperature difference.

[[

]]

[[

]]

Figure 5.1-4. Sensitivity of Fuel Center to Fluid Temperature Difference for 8x8 Fuel

[[

]]

Figure 5.1-5. Sensitivity of Fuel Center to Fluid Temperature Difference for 9x9 Fuel

C3CX Gap Conductance, H

[[

]]

C3DX Direct Moderator Heating, M

The direct moderator heating (DMH) is the energy released into the moderator as the fast neutrons are slowed down. [[

]] The uncertainty in the direct moderator heating is given by the uncertainty in the moderator density, which is determined by the uncertainty in the void fraction (C2AX), and by the uncertainty in the cross section, which is primarily determined by the variation with exposure. The direct moderator heating has been determined based on detailed Monte Carlo calculations with MCNP01A [3]. The DMH model implemented in TRACG accounts for the dependency on moderator density and there is no bias in predicting the mean total amount of direct moderator heating when the default inputs are used. The variation in the direct moderator heating with exposure is not explicitly modeled in TRACG, since, together with all other uncertainties, it results in less than [[ ]] uncertainty in the total amount of DMH. The TRACG model also accurately accounts for how direct moderator heating is distributed in the active channel (in-channel) and in the bypass and water rods (out-channel). This is confirmed by the fact that the uncertainties of the individual components compared to the MCNP predictions are only slightly larger than the uncertainty for the total.

A [[ ]] uncertainty is applied to the total amount of direct moderator heating in order to bound the overall uncertainty in both the amount and the distribution of the direct moderator heating. It is appropriate to consider this uncertainty to be normally distributed as indicated in Reference 3.

C8 Multiple Channel Effect, H

The flow distribution between parallel flow paths such as the fuel channels in the core is controlled by the hydraulic characteristics of the channels. The flow in each individual channel is controlled by the pressure drop components such as static head (given by the void fraction), friction and accelerational pressure drop. Therefore, the uncertainty in the flow in the individual channels and the parallel channel effects are covered by the uncertainty in the interfacial shear and the friction factors. The uncertainty in the interfacial shear is defined in Item C2AX and the uncertainty in friction factors is defined in Item C24.

In addition to the uncertainty in void fraction and friction, the channel pressure drop is dependent on the channel power level and axial distribution. The modeling of the core is derived from the code qualification studies in Reference 2. [[

]]

C10 Void Distribution, H

The uncertainty in the void fraction distribution is included through an uncertainty in the interfacial shear. The uncertainty in interfacial shear is defined in Item C2AX.

C11 Channel – Bypass Leakage Flow, M

The channel leakage flow is based on full-scale measurements for conditions covering the range of expected reactor conditions [22]. [[

]]

C12 Natural Circulation Flows, H

Natural circulation is controlled by a balance between buoyancy and friction. Therefore, the uncertainty in this phenomenon is covered by the uncertainty in interfacial shear (which determines the void fractions) and the uncertainty in the friction factors and form losses. The uncertainty in interfacial shear is defined in Items C2AX, E2 and F1, and the uncertainty in frictional losses is defined in Items A11, C24 and I3.

C23 Water Rod Hydraulics, M

The flow through the water rods is controlled by a calibrated horizontal orifice in the rod. There is a small uncertainty in the loss coefficient. [[

]]

C24 Core Pressure Drop, H

The core pressure drop is composed of static head given by the void fraction, accelerational pressure drop and friction. The uncertainty in the core pressure drop is therefore covered by the uncertainty in the interfacial shear and friction. The uncertainty in interfacial shear is defined in Item C2AX.

TRACG uses the GE design correlation for the wall friction, [[ ]] is based on extensive comparisons to rod bundle pressure drop data [1] from BWR bundles. For single-phase flow in smooth pipes TRACG predicts the pressure drop with an accuracy of [[ ]] For two-phase flow, the majority of the comparisons with the [[ ]] correlation have been made for rod bundle data. Data for GE14 10x10 fuel shows a [[ ]] Based on this data, it is judged that [[ ]] is adequate for all other applications. The components of the flow losses in the fuel bundle and the uncertainty associated with each component are discussed in the following paragraphs.

The side entry orifice and lower tie plate frictional pressure drop is based on full-scale measurements for conditions covering typical reactor operating conditions. The inlet orifice is a sharp-edged orifice with a well-defined flow coefficient. The inlet region upstream of the lower

tie plate has turning losses and a flow expansion at the inlet. The lower tie plate accounts for approximately one third of the total pressure drop. Reference 1 shows that the typical scatter in the loss coefficient for the lower tie plate is of the order of [[ ]] Data from GE's single-phase pressure drop test facility show that the uncertainty for the combined pressure drop for the side entry orifice and the lower tie plate pressure drop is approximately [[ ]], when the entire uncertainty is assigned to the lower tie plate. The exact values for the biases and uncertainties for the 9x9 and 10x10 side entry orifices and lower tie plates are given in Table 5.1-1.

Table 5.1-1:

Bias and Uncertainty in Pressure Drop for 9x9 and 10x10 SEO and Lower Tie Plates

[[

]]

[[

]]

The spacer frictional pressure drop is based on full-scale measurements for conditions covering the range of expected reactor conditions. For 9x9 and 10x10 fuel spacers the uncertainty in the pressure drop for the spacers is determined from full-scale ATLAS data and varies from [[ ]], depending on bundle type. The average uncertainty for all fuel designs is of the order of [[ ]] The bias and uncertainty for current fuel products are given in Table 5.1-2.

Table 5.1-2:

Bias and Uncertainty in Pressure Drop for 9x9 and 10x10 Spacers

[[

]]

The upper tie plate frictional pressure drop is based on full-scale measurements for conditions covering the range of expected reactor conditions. For 9x9 and 10x10 fuel upper tie plates, the

uncertainty in the pressure drop is [[ ]] [51]. The bias and uncertainty for current fuel products are given in Table 5.1-3.

Table 5.1-3:

Bias and Uncertainty in Pressure Drop for 9x9 and 10x10 Upper Tie Plates

[[

]]

Qualification of TRACG against full-scale bundle pressure drop data from the ATLAS facility for an 8x8 bundle with ferrule spacers [2] has shown that TRACG predicts the bundle pressure drop with a bias of [[ ]] and a standard deviation of [[ ]]. These comparisons for total pressure drop are consistent with the above uncertainties for the side entry orifice, lower tie plate, spacers and upper tie plate.

For stability analysis, it is important to vary not only the total pressure drop, but also the single phase and two-phase components separately. Based on the preceding discussion, the following approach will be adopted.

[[

]].

E2 Downcomer Void Profile / Two-Phase Level, H

The downcomer void fraction is determined by the interfacial drag coefficient, C_I. An appropriate uncertainty range for C_I was obtained for large hydraulic diameter regions as discussed below under F1. The downcomer two-phase level is an initial condition depending on the plant operating state. The uncertainty in this parameter is discussed in Section 6.

F1 Chimney and Upper Plenum Void Profile, H

The chimney void distribution is controlled by the interfacial drag coefficient, C_I. An appropriate uncertainty range for C_I was obtained on the basis of TRACG predictions of void fraction data from separate-effects tests by [[

]]. These data are characterized by their applicability to the prediction of void fraction in regions with relatively large hydraulic diameter. Accordingly, they will be used as the basis for defining the uncertainty in interfacial drag in all regions of the reactor except the core and bypass. A statistical summary of the comparisons of TRACG predictions with measurements from these four data sets, combined as a single set of deviations, is shown in Figure 5.1-6. [[

]].

[[

]]. The results are shown in Figure 5.1-7 [[

]].

[[

]]

Figure 5.1-6. Void Fraction Deviations for Tests Applicable to Regions with Large Hydraulic Diameter

[[

]]

Figure 5.1-7. Sensitivity of TRACG Prediction of Average Void Fraction in EBWR Test Facility to PIRT Multiplier on Interfacial Drag Coefficient

[[

]]

Figure 5.1-8 Probability Distribution for Multiplier on Interfacial Drag Coefficient

[[

]].

F6 Interaction between Chimney Cells H

No additional model uncertainties need to be considered for this phenomenon, as it covered by the core, bypass and chimney interfacial and wall shear models, namely C24, B14, F1. [[

]].

I1 Separator Carryunder, M

Separator carryunder affects the core inlet subcooling and hence the decay ratio for stability calculations. Carryunder is calculated by the TRACG separator model. Typical values of carryunder at normal operation are of the order of [[ ]]. An uncertainty of [[ ]].(absolute) bounds the differences between TRACG and separator data and will be used as an estimate of the 1σ uncertainty in the model.

I3 Separator Pressure Drop, H

The loss correlations for the separator pressure drop in TRACG are best fit to two and three stage separator pressure drop data [2]. 95% of the data falls within [[ ]] of the correlation, which has been implemented into TRACG. 95% corresponds to the 2σ level and therefore 6% is a good approximation for the 1σ uncertainty in separator pressure drop.

Table 5.1-4:

Disposition of High and Medium Ranked Stability Model Parameters

[[

]]

5.2 EFFECTS OF NODALIZATION

The nodalization strategy for the various reactor components was developed from the qualification of TRACG against test data for these components. The same consistent nodalization strategy was then applied for full-scale plant calculations. The adequacy of the nodalizations has been demonstrated and supported by sensitivity studies. Standard nodalizations for modeling of BWR reactor vessels and other components have been presented in the *TRACG Qualification Report* [2]

The nodalization for stability involves some refinements in the axial nodalization of the channel component near the boiling boundary and in the channel grouping [2]. This is discussed in more detail below. Also, the ESBWR geometry with the partitioned chimney requires special consideration. [[

]].

5.2.1 VESSEL NODALIZATION FOR ESBWR STABILITY ANALYSIS

Figure 5.2-1 shows the axial and radial nodalization of the ESBWR vessel. The axial levels and radial rings are the same as used previously for AOO analysis for the ESBWR [24], [[

]].

5.2.2 DETAILED NODALIZATION SCHEME FOR THE CHANNEL COMPONENT

[[

]]

5.2.3 CHANNEL GROUPING FOR STABILITY APPLICATIONS

Individual fuel bundles in the core may be modeled in TRACG as individual channels or may be grouped together into a single TRACG channel component. Because of current code limitations within TRACG on the number of components allowed, it is not possible to model every fuel bundle as a single TRACG channel. Consequently, it is necessary to group or combine individual fuel bundles into thermal hydraulic groups. [[

]]

The channels are grouped based on (a) hydraulic considerations to separate hydrodynamic characteristics and (b) neutron kinetics considerations to separate dynamic power sensitivity characteristics.

The channel grouping accounts for additional TRACG capability in the areas of limiting channel response, peripheral channel grouping, and vessel modeling detail. [[

]]

Figure 5.2-4 shows the typical grouping of channel components for stability analysis. [[

]].

[[

]].

Table 5.2-1:
Void Distribution at the Top of the Bypass Region

[[

]]

[[

]]

Figure 5.2-1: Axial and radial nodalization for ESBWR Stability Analysis

[[

]]

Figure 5.2-2: Channel Nodalization Studies from Reference 2

[[

]]

Figure 5.2-3: R- θ Nodalization for ESBWR Stability Analysis

[[

]]

Figure 5.2-4: Channel Grouping for ESBWR Stability Analysis

5.3 EFFECTS OF SCALE

Effects of scale have been specifically addressed as part of the model development as well as the qualification. In the TRACG model description report [1], the ranges of applicability of the basic models and correlations are stated and shown to cover the scale and operating range of BWRs [Table 6.0-1 of Reference 1]. This is a ***necessary*** condition for the validity of TRACG calculations for the full-scale BWR.

The qualification of TRACG [2] covers separate-effects tests, full and reduced scale component performance tests, scaled integral system effects tests, and full-scale BWR plant tests. Accurate predictions of data at various scales (up to a sufficiently large scale) constitute a ***sufficient*** condition for the validity of TRACG calculations for full-scale plants. In general, the qualification results show that both data from scaled test facilities as well as full-scale plant data are well predicted, and that there is no apparent effect of scale in the TRACG calculations.

The conclusion that there is no effect of scale in the TRACG calculations is substantiated in this section.

5.3.1 FULL SCALE TEST COVERAGE

Table 4.2-2 shows the coverage of the Medium and High ranked PIRTs for stability by test data. A number of ESBWR components have been tested at full scale. [[

]].

5.3.2 OPERATING PLANT DATA

Tests performed at BWR plants validate a number of phenomena that are highly ranked for stability. [[

]].

The most relevant and important plant data are the stability measurements that have been made at various BWRs [2]. Data have been obtained for both core wide and regional stability at various plants. [[

]]. The applicability of these data for the ESBWR has been evaluated by comparing the range of important parameters in the plant data with the corresponding ranges for the ESBWR. This comparison is shown in Table 5.3-1.

[[

]]

The void coefficient for ESBWR is at the lower end of the range of operating BWR cores. This results in favorable stability characteristics.

The power to flow ratio (which approximates the average exit quality) for the ESBWR is compared with operating plants in Figure 5.3-1. A line of constant power to flow ratio corresponding to the ESBWR rated conditions is denoted by the dashed line from the origin. The operating plant comparisons are for ABWR and Clinton, at uprated power. The extended operating domain is also shown for both plants. For Clinton, this is the MELLLA+ domain. [[

]].

The radial peaking for the ESBWR core is similar to that for operating plant cores. Thus, the comments for average power-to-flow ratio apply to the hot bundle power to flow ratio.

[[

]]

The ratio of single phase to two-phase pressure drop in the ESBWR core is similar to, but more favorable than, that for operating BWRs.

In summary, TRACG has been validated over a range of plant stability data and no additional uncertainty is needed to account for scale-up effects.

Table 5.3-1:

Range of Key Stability Parameters - ESBWR vs. Operating Plant Data

[[

]]

[[

]]

Figure 5.3-1: Comparison of Power and Flow per Bundle for ESBWR vs. Operating BWRs

[[

]]

Figure 5.3-2: Variation in Harmonic Sub-criticality vs. Core Size

5.4 SENSITIVITY ANALYSIS

Sensitivity studies have been performed, varying each highly ranked model parameter from -1σ to $+1\sigma$. These results are shown in Section 8. These studies serve to identify the parameters that have the largest impact on the calculated safety parameters (decay ratios).

6.0 APPLICATION UNCERTAINTIES AND BIASES

Code inputs can be divided into four broad categories: (1) geometry inputs, (2) model selection inputs, (3) initial condition inputs, and (4) plant parameters. For each type of input, it is necessary to specify the value for the input. If the calculated result is sensitive to the input value, then it is also necessary to quantify the uncertainty in the input.

The geometry inputs specify lengths, areas and volumes. Uncertainties in these quantities are due to measurement uncertainties and manufacturing tolerances. These uncertainties usually have a much smaller impact on the results than do uncertainties associated with the modeling simplifications.

Individual geometric inputs are the building blocks for the spatial nodalization. The spatial nodalization includes modeling simplifications such as the lumping together of individual elements into a single model component. For example, several similar fuel channels are lumped together and simulated as one fuel channel group. An assessment of these kinds of simplifications, along with the sensitivities to spatial nodalization, is included in the TRACG Qualification LTR [2].

Inputs are used to select the features of the model that apply for the intended application. Once established, these inputs are fully specified in the procedure for the application and do not change.

A plant parameter is defined as a plant-specific quantity such as a protection system scram characteristic, etc. Plant parameters influence the characteristics of the transient response and have essentially no impact on steady-state operation.

Initial conditions are those conditions that define a steady-state operating condition. Initial conditions may vary due to the allowable operating range or due to uncertainty in the measurement at a given operating condition. The plant Technical Specifications and Operating Procedures provide the means by which controls are instituted and the allowable initial conditions are defined. At a given operating condition, the plant measurement system has inaccuracies that also must be accounted for as an uncertainty.

6.1 KEY INITIAL CONDITIONS AND PLANT PARAMETERS

Table 6.1-1 lists the key plant initial conditions that are high ranked for the stability application. There are no plant parameters that are relevant to the stability analysis. The second column describes how the initial conditions are controlled during operation. The uncertainty is specified in Column 3. The 'Comments' column indicates the "PIRT" parameters that are varied for the TRACG analysis. These are special inputs that allow coefficients in TRACG correlations to be varied for the purpose of uncertainty analysis.

Table 6.1-1:
Key Plant Initial Conditions

[[

]]

Table 6.1-1 Notes

[[

]]

7.0 COMBINATION OF UNCERTAINTIES

A proven Monte Carlo technique is used to combine the individual biases and uncertainties into an overall bias and uncertainty. The Monte Carlo sample is developed by performing random perturbations of model and plant parameters over their individual uncertainty ranges. Using the histogram generated by the Monte Carlo sampling technique, a probability density function is generated for code output of the primary safety criteria parameters. The determination of decay ratio with TRACG is a two-step process. The Monte Carlo trials produce a distribution of plant initial conditions. The decay ratio for each initial condition is then obtained by examining the response to a pressure or flow impulse function. The probability distribution function of decay ratios thus includes the variability in the initial conditions as well as the transient response.

In order to determine the total uncertainty in predictions with a computer code, it is necessary to combine the uncertainties due to model uncertainties (CSAU Step 9), scaling uncertainties (CSAU step 10), and plant condition or state uncertainties (CSAU Step 11). Various methods have been used to combine the effects of uncertainties in safety analysis. This section briefly summarizes different methods for combining uncertainties. All these approaches are within the framework of the CSAU methodology, since the CSAU methodology does not prescribe the approach to use. The method for combining uncertainties that is used for application to ESBWR stability analyses is the same approach that has been successfully used and approved by the NRC for the analyses of AOO transient scenarios [3].

7.1 TRADITIONAL BOUNDING ANALYSIS

A commonly used approach in traditional conservative analysis is to combine the uncertainties linearly, by taking bounding models for the phenomena and by setting plant parameters to limits expected to produce the most limiting plant response. Separate calculations may be required to obtain bounding results for different response parameters, because it may not be possible to define a single 'worst case' that will result in all key response or output parameters being calculated at their upper bounds. In any case, an advantage of this approach is that it requires no more than one computer run for each output parameter of interest. The most significant disadvantages with this method are that it is very conservative, in extreme cases can give unrealistic results; and no statistical quantification of the margins to design limits is possible. This bounding approach has historically been used for stability analysis.

7.2 STATISTICAL TREATMENT OF OVERALL CALCULATIONAL UNCERTAINTY

An improved approach employs realistic plant calculations for the evaluation of the primary safety criteria using realistic models and nominal input for the plant parameters. An uncertainty is then added on to the calculated primary safety parameters to account for modeling uncertainty, uncertainty in plant operation and state, and other effects such as effect of scale on the calculations. A statistical approach is used to determine the added uncertainty on top of the nominal calculation. Realistic models and input are used for all processes and inputs, and the design calculation accounts for uncertainties in all major models and plant parameters.

7.3 COMPARISON OF APPROACHES FOR COMBINING UNCERTAINTIES

Several options exist to perform the statistical combination of the uncertainties. Neither the CSAU methodology report [8] nor NRC Regulatory Guide 1.157 [9] specifies how this should be done. Some possible options are summarized in Table 7.3-1.

These options are discussed and compared in the following paragraphs. [[

]]

Table 7.3-1:

Methods for Combining Uncertainty

Method	Description
Propagation of Errors	Uncertainties in the calculated safety parameters to individual phenomena are evaluated from single perturbations and the overall uncertainty is determined as the square root of the sum of the square of the individual uncertainties.
Response Surface Technique	Response surface for the safety parameter is generated from parameter perturbations. Statistical upper bound value determined from Monte Carlo Method using response surface.
Order Statistics (OS) Method - Single Bounding Value	Monte Carlo Method using random perturbations of all important parameters. Statistical upper bound determined from most limiting perturbation (for first order statistics).
[[ ]]	[[ ]]

7.3.1 PROPAGATION OF ERRORS

In the Propagation of Errors method, the uncertainties are combined by taking the square root of the sum of the squares (SRSS) of the individual uncertainties. In this approach, the effects of individual phenomena on key response parameters are determined, and then combined using SRSS. For this approach, a relatively small number of computer runs is required. The number of runs required is directly related to the number of input parameters for which uncertainty ranges have been established. This approach is justifiable if the effects on the calculated responses of the phenomena whose uncertainties are being accounted for are independent of each other. For complex processes requiring complex code calculations, independence rarely exists and is difficult to demonstrate. A secondary requirement for this approach is that all input and output parameters can be modeled by a normal distribution.

7.3.2 RESPONSE SURFACE TECHNIQUE

In this method, individual model and plant parameters are perturbed and the sensitivity of the primary safety parameter to these perturbations is determined. The process begins by examining each model and plant parameter uncertainty. Using test data and expert knowledge, each parameter is assigned a probability density function (i.e., normal, log normal, exponential, uniform, etc.). The probability density function (PDF) describes the method by which the uncertainty would vary from the expected value. The range for each PDF is determined from the standard deviation, if known, or by the maximum and minimum value of the parameter. As an example, the uncertainty in fuel conductivity is distributed normally with a nominal (mean) value of 0 % and a standard deviation of 13%. According to conventional response surface techniques, a large number of transient simulations per each event scenario would be needed due to the large number of parameters to be varied. At least two cases would be required (in addition to the nominal calculations) for each important plant and model parameter to quantify the responses to $\pm\sigma$ perturbations. Additional cases would be needed to quantify $\pm 2\sigma$ and $\pm 3\sigma$ perturbations if the output responses did not vary linearly with the input perturbations. Furthermore, many cases would have to be made, where several parameters are perturbed simultaneously to account for covariances. A response surface would be determined from all the cases, and Monte Carlo analysis would be used to determine the 95% fractile. This method is advantageous when few parameters are involved, but is impractical when a large number of parameters are involved due to the prohibitively large number of perturbations needed to account for non-linearities and covariances.

In the PIRTs in Section 3, over 20 high and medium ranked phenomena are identified that would need to be treated statistically. Assuming one input parameter per phenomena and ignoring other uncertainties associated with initial conditions and plant parameters, it is possible to estimate how many calculations are required. To run the base case, the $\pm 1\sigma$, $\pm 2\sigma$, and $\pm 3\sigma$ perturbations would require over 120 transient simulations per event scenario. Similarly, an even larger number of calculations would be needed to evaluate covariances. However, an important advantage is that single parameter perturbations provide useful insight by identifying the most sensitive parameters.

7.3.3 ORDER STATISTICS (OS) METHOD – SINGLE BOUNDING VALUE

The Monte Carlo method that has been used in Germany by Gesellschaft für Anlagen-und Reaktorsicherheit (GRS) [32] and for the application of TRACG to AOOs by GE [3] requires only a modest number of calculations, and automatically includes the effects of interactions between perturbations to different parameters. In the OS method, Monte Carlo trials are used to vary all uncertain model and plant parameters randomly and simultaneously, each according to its uncertainty and assumed probability density function (PDF), and then a method based on the order statistics of the output values is used to derive upper tolerance bounds (one-sided, upper tolerance limits OSUTLs).

Monte Carlo sampling of each parameter according to its assigned PDF yields the value of that parameter to be used for a particular trial. Given such a trial set of input parameters, the calculation process determines the corresponding output parameter of interest. Therefore, while the void coefficient might be set at a -1.5σ value, interfacial shear might be set to a value of +2.0σ, each according to its own probability model. In this manner, the effects of interactions between all model parameters are captured in a single calculation. Once all of the trials have been completed, the desired output parameter (e.g., decay ratio) is extracted from each of the trials and the set of parameter values is then used to construct an OSUTL for that particular output parameter. Figure 7.3-1 illustrates this process.

[[

]].

An OSUTL is a function $U = U(x_1,\ldots,x_n)$ of the data $x_1,\ldots,x_n$ (which will be the values of an output parameter of interest in a set of Monte Carlo trials), defined by two numbers $0 < \alpha, \beta < 1$, so that the proportion of future values of the quantity of interest that will be less than U is 100α%, with confidence at least 100β% --- this is called an OSUTL with 100α%-content and (at least) 100β% confidence level.

The order statistics method, originally developed by Samuel Wilks, produces OSUTLs that are valid irrespective of the probability distribution of the data, requiring only that they be a sample from a continuous PDF. [[

]]

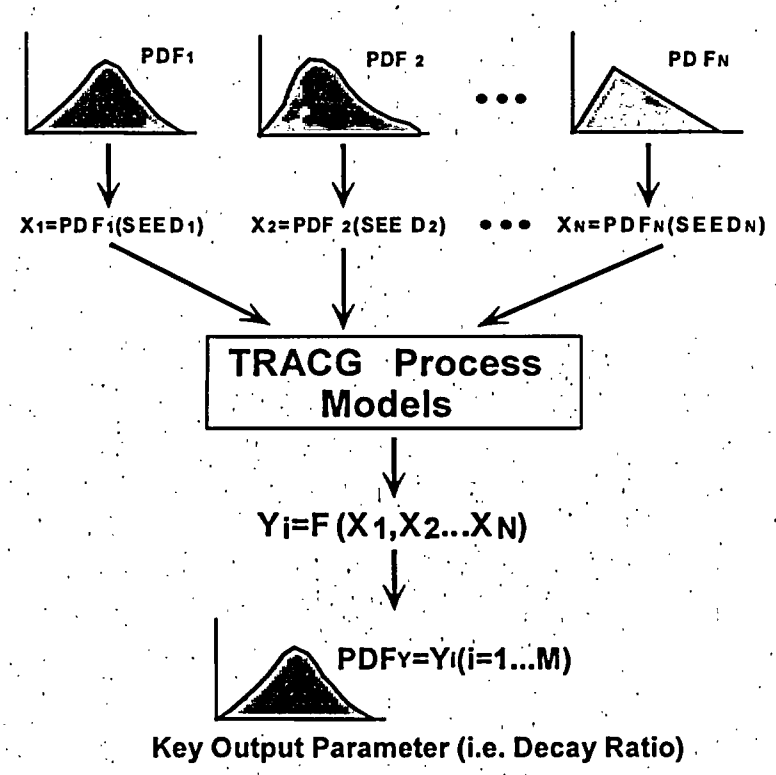

Figure 7.3-1. Schematic Process for Combining Uncertainties

7.3.4 NORMAL DISTRIBUTION ONE-SIDED UPPER TOLERANCE LIMIT

[[

]]

7.4 RECOMMENDED APPROACH FOR COMBINING UNCERTAINTIES

[[

]].

This approach to determine the total uncertainty has several advantages over other approaches as summarized in Table 7.4-1. The following expands on the discussion of these advantages:

[[

-

]].

- A separate response surface does not have to be developed for each output parameter of interest.
- It allows for different specifications of the distributions of the uncertainties: for example, some can be specified as having a uniform distribution and some can be specified with a normal distribution. (This advantage is not unique to this method: Monte-Carlo sampling with a response surface will also allow this.)

[[

]]

Table 7.4-1

Comparisons of Methods for Combining Uncertainties

Method for Combining Uncertainties	Advantages	Disadvantages
Propagation of Errors	Relatively small number computer runs, when the number of input variables is small. The number of cases is linearly related to the number of input parameter uncertainties considered.	Approximate, because it involves linearization. Necessary to demonstrate independence of effects of individual uncertainties on responses, or else must include covariances explicitly.
Response Surface	Very precise statistical characterization of results can be achieved with a large number of Monte Carlo Trials using response surface. Different distributions can be specified for each input uncertainty. Independence of the effect of individual input parameters on response is not necessary.	Number of computer runs depends on the response surface model and increases exponentially with the number of input parameter uncertainties considered. A separate response surface must be fitted for each output variable of interest. Interactions between input parameters have to be established and considered in the development of the response surface.
[[		]].
[[		]].

7.5 IMPLEMENTATION OF STATISTICAL METHODOLOGY

The purpose of this section is to describe the process by which the statistical results will be used to (1) determine decay ratios for channel stability and core wide stability, and (2) establish that these safety parameters have acceptable margins to design limits.

[[

]].

7.5.1 CONFORMANCE WITH DESIGN LIMITS

The method described in Section 7.4 is applied in the following process. The number of trials may be increased to increase the confidence level for the statistical analysis.

- Identify all High and Medium ranked parameters uncertainties from Section 5 for the stability type to be analyzed. These parameters will be utilized in the statistical analysis.

  [[

]]

8.0 DEMONSTRATION ANALYSES

This section presents sample results to demonstrate the application methodology for ESBWR stability analysis. Calculations made on a nominal best-estimate basis are termed "Baseline Analysis" results. These calculations are made for channel and core decay ratios. Nominal regional decay ratios are also calculated. The purpose of the regional decay ratio calculations is to provide confidence in the approach of using the channel and core-wide decay ratio map for licensing analysis.

Sensitivity studies are performed to examine the effects of the High and Medium ranked parameters on the channel and core-wide decay ratios. Uncertainties are statistically combined for the channel and core-wide decay ratios with the Monte Carlo technique discussed in Section 7. These values are compared against the design limits at the 2σ confidence level.

8.1 BASELINE ANALYSIS

The ESBWR plant has 1132 bundles and a rated thermal power of 4500 MWt. The vessel modeling is illustrated in Figure 8.1-1 and Figure 8.1-2. The plant has an equilibrium core of GE14 10x10 fuel. Figure 8.1-2 also shows the average bundle power in the various core sectors. The bundles in Ring 3 are grouped into two groups, with the bundles with inlet orificing corresponding to the peripheral region having a much lower average power level. Figure 8.1-3 illustrates the TRACG core map showing the thermal hydraulic channel groups. The number of channels in each thermal hydraulic group and the peaking factors for each group are shown in Table 8.1-1. Channel groups were created based on core position, chimney position, orifice geometry, and peaking factor. [[

]]

A sensitivity study was performed by further subdividing the larger groups based on channel power differences. The results (reported in Section 8.1.2.2) showed very little sensitivity and confirm that the chosen grouping is adequate for representing the ESBWR core for stability analysis.

Analysis was conducted at various points in the cycle: Beginning of Cycle (BOC), Middle of Cycle (MOC) near the peak reactivity state, and End of Cycle (EOC). Figure 8.1-4 shows the core average axial power profiles at these exposures. [[

]]

[[

]]

A baseline analysis was performed for the ESBWR at rated conditions, which are the most limiting from the perspective of stability due to the highest power/flow ratio. In addition, Anticipated Operational Occurrences (AOOs) that could lead to more severe conditions of power and flow were also examined. Figure 8.1-7 shows the natural circulation operating curve for the ESBWR. Two transients can lead to more limiting states for stability. A Loss-of-Feedwater (LOFW) event will lead to a drop in the level until a scram occurs on low level (Level 3). The lowest level and correspondingly, the lowest core flow are reached just prior to scram. The power/flow trajectory for this transient is shown in Figure 8.1-7. The end point is determined by the Level 3 scram, and leads to a more severe power/flow ratio than at rated conditions. A Loss-of-Feedwater Heater (LOFWH) transient results in an increase in power due to the reactivity addition by the colder feedwater. The event is terminated by a scram on high thermal power. The trajectory for this transient is also shown in Figure 8.1-7. The highest power/flow ratio is reached just prior to the scram.

8.1.1 CHANNEL STABILITY RESULTS

Channel stability analysis was performed by perturbing the flow to the high power channels while keeping the power constant. The calculation process is as follows:

[[

]]

8.1.1.1 SUPER BUNDLE STABILITY

[[

]]

8.1.2 CORE WIDE STABILITY RESULTS

Core stability was evaluated at BOC, MOC and EOC conditions. The calculations were made with the 3-D kinetics model interacting with the thermal hydraulics parameters. The calculation sequence is as follows:

[[

]]

8.1.2.1 SENSITIVITY TO METHOD OF PERTURBATION

[[

]]

8.1.2.2 SENSITIVITY TO CHANNEL GROUPING

[[

]]

8.1.3 REGIONAL STABILITY RESULTS

[[

]]

Table 8.1-1:
TRACG Channel Grouping (MOC)

[[

]]

Table 8.1-2:

Higher Harmonic Mode Sub-criticality at Different Exposures

[[

]]

Table 8.1-3:

Initial Conditions for Channel and Core Stability Analysis

[[

]]

Table 8.1-4:
Initial Conditions for Super Bundle Stability Analysis

[[

]]

Table 8.1-5:
Regional Stability: Decay Ratio by Subgroup

[[

]]

[[

]]

Figure 8.1-1. TRACG ESBWR Vessel R-Z Modeling

[[

]]

Figure 8.1-2: R-θ Nodalization of ESBWR Core Region showing Average Power (MW) in Each Region

[[

]]

Figure 8.1-3: TRACG Channel Grouping for ESBWR Core

[[

]]

Figure 8.1-4: Core Average Axial Power Shape at Different Exposures

[[

]]

Figure 8.1-5: Flux Distribution for First Azimuthal Harmonic with Axis of Symmetry

[[

]]

Figure 8.1-6: Flux Distribution for Second Azimuthal Harmonic with Axis of Symmetry

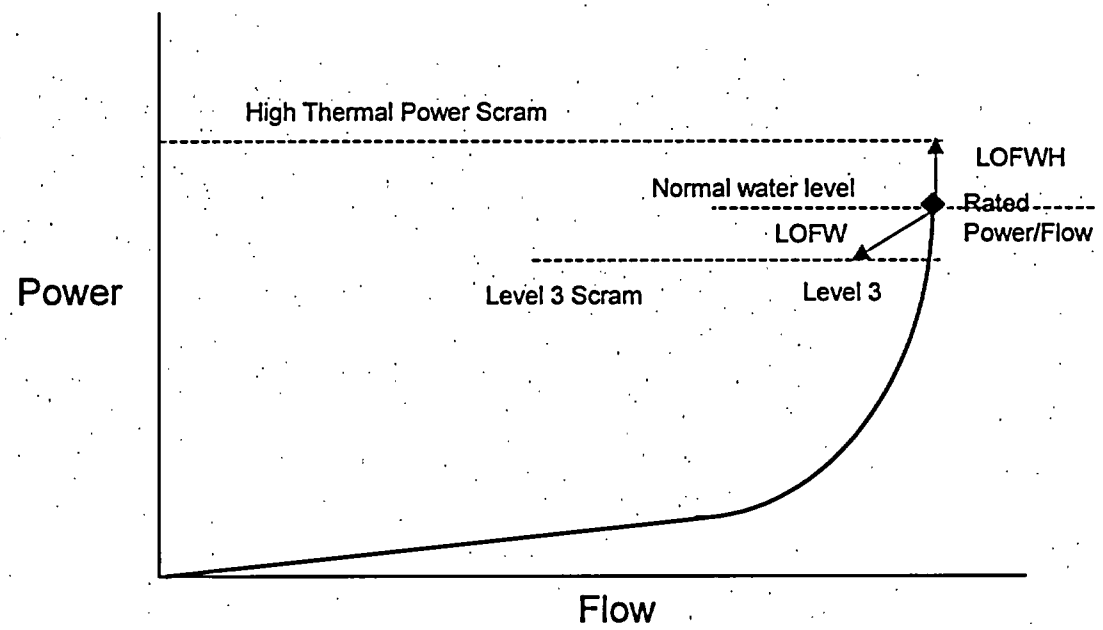

Figure 8.1-7: ESBWR Natural Circulation Operation with Limiting Conditions for Stability Analysis

[[

]]

Figure 8.1-8: Hot Bundle Flow Response to Transient Inlet Flow Perturbation

[[

]]

Figure 8.1-9: Hot Super Bundle Flow Response to Transient Inlet Flow Perturbation

[[

]]

Figure 8.1-10: Core Power Response to Transient Turbine Inlet Pressure Perturbation

[[

]]

Figure 8.1-11: Sensitivity to Perturbation Size

[[

]]

Figure 8.1-12: Power Distribution by Channel in Large Sectors in Ring 1

[[

]]

Figure 8.1-13: Power Distribution by Channel in Large Sectors in Ring 2

[[

]]

Figure 8.1-14: Finer Channel Grouping by Power Level

[[

Figure 8.1-15: Sensitivity to Detailed Channel Grouping]]

[[

]]

Figure 8.1-16: Power Distribution for First Harmonic

[[

]]

Figure 8.1-17: Core Map showing Products of Fundamental and First Harmonic Powers (Regions with highest absolute values are shown in dark brown)

[[

]]

Figure 8.1-18: Channel Grouping for Regional Stability Calculation (darker colored regions have higher absolute peaking)

[[

]]

Figure 8.1-19: Channel Power Responses to Out-of-Phase Flow Perturbation

[[

]]

Figure 8.1-20: Symmetrically Located Channel Power Responses to Out-of-Phase Flow Perturbation

8.2 SENSITIVITIES TO HIGH AND MEDIUM RANKED PARAMETERS

Sensitivity studies were performed for the High and Medium ranked PIRT parameters from Table 4.2-2. The parameters were ranged to their $\pm$ 1σ levels for the normally distributed parameters, and to the ends of their expected range for the others. [[

]]

8.2.1 CHANNEL DECAY RATIO

[[

]]

Table 8.2-1 shows the sensitivity study results. The physical parameter varied is shown in the first column with (H) in parentheses if it was ranked High. The "PIRT Multiplier" in TRACG is shown in the second column; the suffix M denotes a reduction in the multiplier (relative to the nominal value of 1) and the suffix P denotes an increase. (The feedwater enthalpy is changed via input). The range of variation is shown in the next column. The sensitivity in channel decay ratio is shown in the last column. [[

]]

8.2.2 CORE DECAY RATIO

[[

]]

Table 8.2-2 shows the sensitivity study results for the core decay ratio. The columns in the table are the same in Table 8.2-1. The additional parameters included are the void coefficient and the fuel conductivity. [[

]]

Table 8.2-1:

Sensitivity of Channel Decay Ratio to High and Medium-Ranked PIRT Parameters

[[

]]

Table 8.2-2:

Sensitivity of Core Decay Ratio to High and Medium-Ranked PIRT Parameters

[[

]]

8.3 STATISTICAL ANALYSIS OF ESBWR STABILITY

Monte Carlo analyses were performed to assess the uncertainty in the calculation of the core and channel decay ratios associated with the model and application uncertainties (Sections 5 and 6). The probability distributions obtained from the Monte Carlo trials are used to estimate the One-Sided Upper Tolerance Limits (OSUTL) that bound 95% of the content with 95% confidence as discussed in Section 7.

8.3.1 CHANNEL DECAY RATIO STATISTICAL ANALYSIS

[[

]]

8.3.2 CORE WIDE DECAY RATIO STATISTICAL ANALYSIS

[[

]]

8.3.3 COMPARISON WITH DESIGN LIMITS

In Section 2.2, design requirements were established for the channel and core decay ratio. Figure 8.3-8 shows the stability map with the design criteria. [[

]]

Table 8.3-1:
Parameters and Distributions for Monte Carlo Trials

[[

]]

[[

]]

Figure 8.3-1: Monte Carlo Trials for Channel Decay Ratio

[[

]]

Figure 8.3-2: Monte Carlo Results for Channel Flow

[[

]]

Figure 8.3-3: Monte Carlo Results for Channel Decay Ratio

[[

]]

Figure 8.3-4: Monte Carlo Trials for Core Decay Ratio

[[

]]

Figure 8.3-5: Correlation between Core Decay Ratio and Power/Flow Ratio

[[

]]

Figure 8.3-6: Monte Carlo Results for Core Flow

[[

]]

Figure 8.3-7: Monte Carlo Results for Core Decay Ratio

[[

]]

Figure 8.3-8: Decay Ratio Results Compared to Design Criteria

8.4 STABILITY FOLLOWING ANTICIPATED OPERATIONAL OCCURRENCES (AOOS)

The rated power and flow conditions are the limiting conditions for stability for the ESBWR during normal operation. However, following an AOO the power/flow conditions could be more severe than at rated. Two AOOs were identified in Section 2.2: Loss-of Feedwater Heater (LOFWH), which results in increased power; and Loss of Feedwater Flow (LOFW), which results in a lower flow. The trajectories of the transients in the power – flow map are shown in Figure 8.4-1. The curve A-A corresponds to operation with a reduced level in the downcomer. The lower level leads to a reduction in flow. Different points on A – A correspond to changes in control reactivity or changes in core inlet subcooling.

LOFWH is a slow transient, in which the power increases slowly as the feedwater temperature drops. If no action is taken by the operator, the power would increase until a high thermal power scram occurs at 115% of rated power. [[

]]

Channel stability was also analyzed at this pre-scram power level. Figure 8.4-4 shows the response of the channel inlet flow following an instantaneous perturbation of [[ ]] The decay ratio was calculated to be [[ ]] at rated conditions.

Analysis of the LOFW transient turned out to be more complex. The transient is rapid and unless the feedwater flow is restored, will scram in a few seconds on a trip at L3. In this period, the flow, power and subcooling are dropping and pressure is responding to the pressure controller. Rather than imposing a pressure perturbation on top of the transient response to evaluate the decay ratio, the following approach was adopted. [[

]] This operating point is more severe than the rated

condition as the flow is reduced at the same power level. It provides a conservative evaluation of the LOFW transient, as the power is higher than would occur during a LOFW.

Results of core stability analysis for the reduced level case are shown in Figure 8.4-5. The core decay ratio was evaluated to be [[ ]] The hot channel stability was also evaluated by perturbing the inlet velocity. The resulting transient response is shown in Figure 8.4-6. The hot channel decay ratio increased from [[ ]] at rated conditions to [[ ]] for the reduced level case.

The results from these studies show that adequate margin is maintained to the stability design criteria even for these more severe operating states.

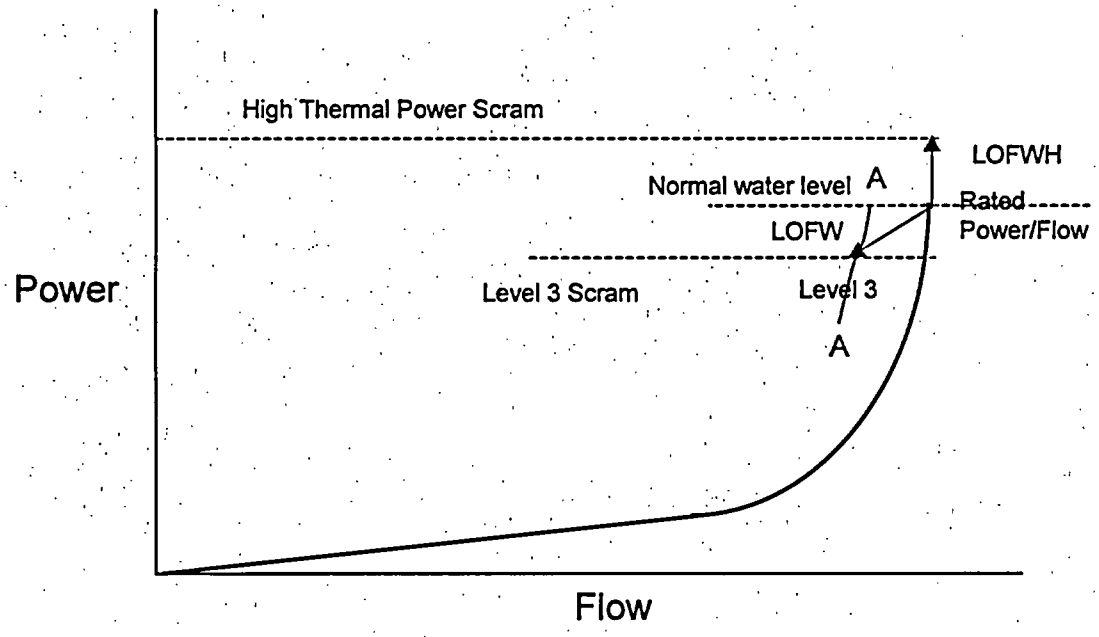

Figure 8.4-1: Stability in Expanded Operating Map

[[

]]

Figure 8.4-2: Loss of Feedwater Heater Transient

[[

]]

Figure 8.4-3: Core Power Response to Pressure Perturbation (Scram Power Level)

[[

]]

Figure 8.4-4: Hot Channel Flow Response to Inlet Flow Perturbation (Scram Power Level)

[[

]]

Figure 8.4-5: Core Power Response to Pressure Perturbation at Reduced Level

[[

]]

Figure 8.4-6: Hot Channel Response to Inlet Flow Perturbation at Reduced Level

9.0 PLANT STARTUP

In contrast to operating BWRs, the ESBWR plant starts up without recirculation pumps. At low pressure, the initiation of voiding in the core and chimney causes perceptible changes in the driving head because of the large difference between liquid and vapor densities. Consequently, startup procedures are developed to assure smooth ascension in pressure and power.

Tests in experimental natural circulation loops [26], [27], [35] have identified two mechanisms for potential flow oscillations at low pressure. First, at very low flows, a periodic "geysering" flow oscillation was found to occur due to condensation of core exit vapor in the subcooled chimney region. Condensation–induced oscillations may occur under these conditions. The condensation rate is determined by the chimney subcooling and the rate of vapor production in the core. Oscillations of this kind are unlikely given the ESBWR startup procedures, which are similar to those of the natural circulation Dodewaard reactor. Dodewaard experienced no "geysering" oscillation in its 22 refuel cycles of operation. Second, initiation of vapor production in the chimney region leads to a reduction in hydrostatic head in the chimney and a resultant core flow increase. This, in turn, could cause voids to collapse in the chimney, leading to a reduction in flow. Oscillations of this second kind (known in the literature as Type 1 instability [28], see Figure 9.1-1) had also never been seen at Dodewaard. In the final cycle of its operation, a special startup test was performed to probe the low-pressure portion of the startup trajectory. Though no oscillations were detectable on the APRMs, it was possible to infer the presence of small oscillations in core velocity from the auto correlation function of the APRM signal (Figure 9.1-2) [29]. These were small oscillations superposed on the core velocity with little, if any, reactivity impact, as the core flow is single phase in this phase of the startup transient.

In this section, the mechanism of the hydrostatic oscillations is examined and startup trajectories are analyzed with TRACG. The results show that large margins to boiling transition are maintained throughout the startup scenario.

9.1 PHENOMENA GOVERNING OSCILLATIONS DURING STARTUP

During startup, the water in the ESBWR vessel is initially heated to about 85 C by decay heat supplemented by auxiliary heaters. The ESBWR design is not finalized, but one concept for auxiliary heating is to use the Reactor Water Cleanup (RWCU)/ Shutdown Cooling (SDC) system. Following de-aeration, control rods are pulled to criticality and nuclear heatup begins at a low core power. As the water circulates through the core and downcomer by natural circulation, it is gradually heated up. The RWCU system removes a portion of the heat by draining water from the downcomer and lower plenum, cooling it in heat exchangers and returning it through the feedwater sparger. Because of the large height of the ESBWR vessel, the pressure at the water level (near the top of the separators) is lower than the core pressure by about 1 bar. Figure 9.1-3 shows a schematic of the vessel and the axial pressure profile. At low pressures corresponding to startup conditions, the pressure gradient gives rise to a significant difference in the saturation temperature between the core exit and the top of the separators. The saturation temperature profile is shown on the right side of the figure. As the circulating water is

slowly heated up, saturation temperature is first reached at the top of the separators. Vapor generation at the top of the separators results in a reduction in the density head in the separators, and the voids propagate downwards. The formation of voids also results in a larger driving head for natural circulation flow. The increase in natural circulation flow reduces the core exit temperature and leads to a collapse of the voids. This completes one cycle of the hydrostatic head oscillation. The sequence of events for one cycle is illustrated in the right hand portion of Figure 9.1-3. These oscillations persist until the inlet temperature to the core increases and a steady void fraction is established in the separators. Small oscillations in the flow rate are harmless when the flow in the core is single phase and consequently there is a very large margin to thermal limits. This type of oscillation is termed Type 1 instability in the literature.

Figure 9.1-1 is a schematic of a generalized stability map in the plane of Subcooling Number vs. Zuber Number. (The figure does not represent a quantitative stability map specifically for the ESBWR and is used primarily for illustrative purposes.) Two different boundaries are shown for core-wide (in-phase) and regional (out-of-phase) oscillations that have been covered earlier in this report. These are driven by density wave oscillations and are known as Type 2 oscillations. The region above the lower (out-of-phase) stability boundary curve is unstable; the region under the curve is stable. The Type 1 oscillations appear at the onset of voiding and occupy a narrow region next to the line that demarcates the single-phase region from the two-phase region. At normal conditions the ESBWR is very stable as shown in the figure, with significant margin to the stability boundary. During startup, the Type 1 instability region has to be crossed to get to rated pressure and power. It is best to cross the Type 1 instability region at low power before boiling starts in the core to maintain a large margin to thermal limits. Once steady voiding is established in the separators and chimney, the core power can be raised along a trajectory to full power.

The parameters that control Type 1 instability are the Zuber Number and Subcooling Number. The Froude Number is a parameter that is relevant in determining the relationship between the riser buoyancy and the circulation flow. This is important in establishing a scaling basis for tests facility design, but not for loop stability once the scaled flow characteristics are known. Another group that is important for tall columns of liquid at low system pressure is the Flashing Number. These dimensionless numbers are defined below:

$$
\begin{aligned}
N_{Zu} &= \frac{\rho_l}{\rho_{gsd}} \frac{Q}{W_c h_{fg}} \\
N_{sub} &= \frac{\rho_l}{\rho_{gsd}} \frac{(h_{fsd} - h_{in})}{h_{fg}} \\
N_{Fr} &= \frac{V_c^2}{gH_{dc}} \\
N_{fl} &= \frac{\rho_l}{\rho_{gsd}} \frac{(h_{fin} - h_{fsd})}{h_{fg}}
\end{aligned}
\tag{9.1}
$$

where

ρ =density (kg/m^3)

V_c = core average inlet velocity (m/s)

Q =core thermal power (kW)
W_c =core flow (kg/s)
h = enthalpy (kJ/kg)
h_f = saturated liquid enthalpy (kJ/kg)
h_{fg} =latent heat of evaporation at steam dome pressure (kJ/kg)
H_{dc} = downcomer height (m)
sd denotes properties at the steam dome pressure and *in* denotes properties at the inlet to the core.

The significance of these quantities is discussed below with the aid of Figure 9.1-4.

The Zuber Number is a measure of the enthalpy increase in the core. As there is no increase in the enthalpy in the chimney, the Zuber number is also a measure of the total enthalpy increase in the core and chimney regions. The Flashing Number has special relevance for tall columns of liquid at low pressure. It is a measure of the enthalpy margin to flashing at the core exit (see Figure 9.1-4) when the flow just reaches saturation at the top of the chimney. The Subcooling Number is a measure of the enthalpy margin to saturation at the core inlet. At low system pressures, the definition of the Subcooling Number must be considered carefully because of the difference in pressure at different elevations. In Eq. 9.1, it is defined with respect to the saturated enthalpy at the steam dome pressure.

With the above definitions, when saturated conditions are reached at the top of the riser (Path A in Figure 9.1-4), an energy balance leads to:

$$N_{Zu} = N_{sub} \tag{9.2}$$

For Type 1 oscillations that occur when voiding begins at the top of the riser, N_{sub} is the relevant parameter to be used in the stability map of Figure 9.1-1.

For a rapid heatup rate corresponding to Path C in Figure 9.1-4, saturated conditions may be reached at the top of the core (i.e. at a pressure close to core inlet pressure) with a subcooled chimney. In the extreme case when the entire chimney is still subcooled:

$$N_{Zu} = N_{sub} + N_{fl} \tag{9.3}$$

These heatup rates can lead to condensation-induced oscillations. A large flashing number will require a correspondingly higher Zuber number (enthalpy increase in the core) to trigger such oscillations and thus provides a buffer to the occurrence of this phenomenon.

At intermediate conditions, as the void initiation location moves down into the chimney,

$$N_{sub} < N_{Zu} < (N_{sub} + N_{fl})$$

This corresponds to Path B in Figure 9.1-4.

Values of these parameters during the startup of the ESBWR are discussed further in Section 9.2.

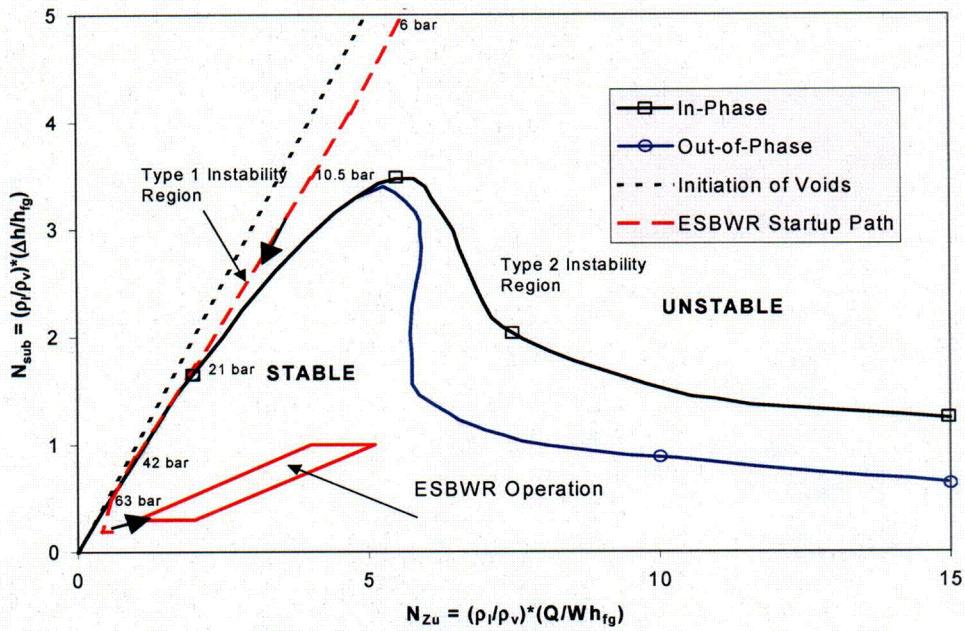

Figure 9.1-1: Generalized Stability Map showing Type 1 and Type 2 Instability [28]

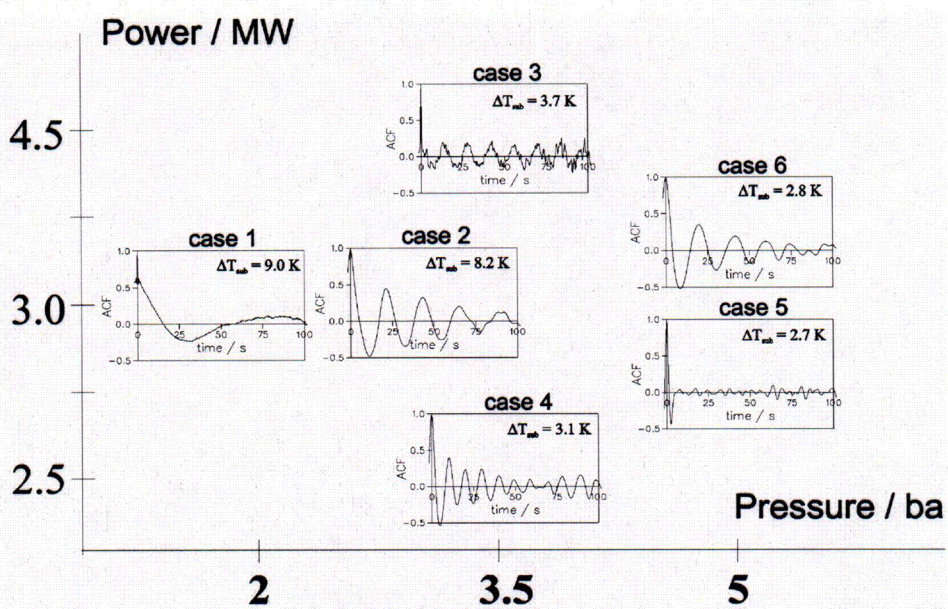

Figure 9.1-2: Indications of Periodic Behavior during Dodewaard Startup [29]

C-02

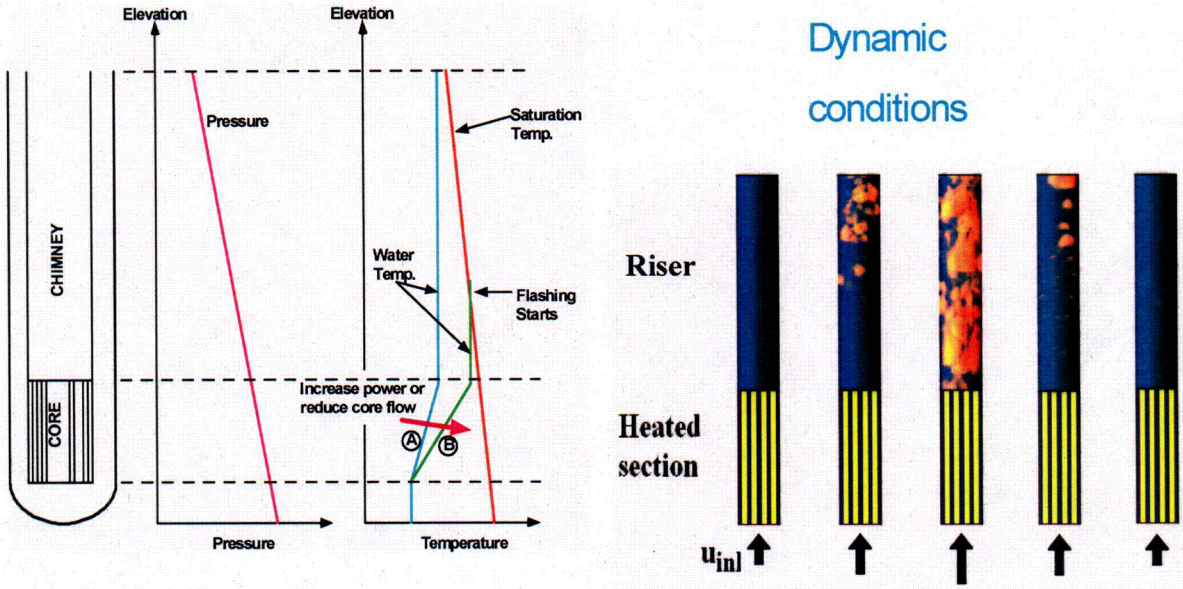

Figure 9.1-3: Thermal – Hydraulic Conditions during Startup [28]

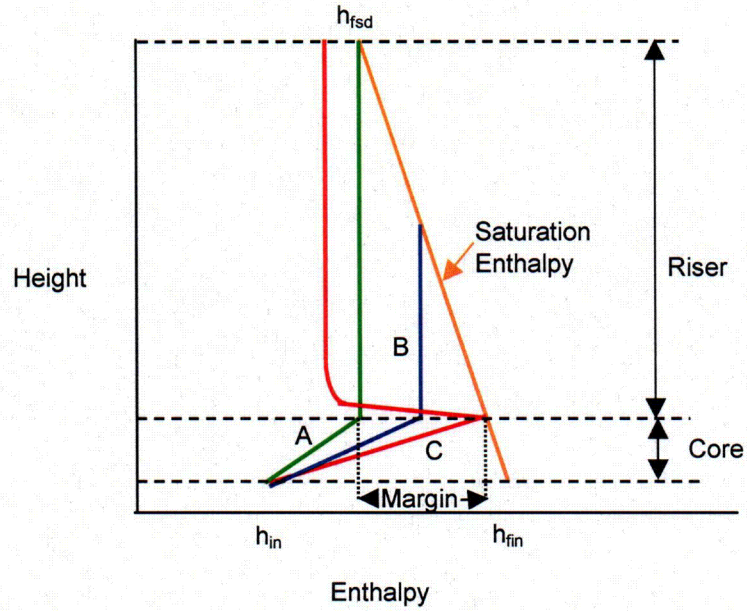

Figure 9.1-4: Enthalpy Profiles for Different Heatup Rates

C-03

9.2 APPLICABILITY OF TRACG FOR STARTUP CALCULATIONS

A PIRT was developed for density wave oscillations in Section 3. No new phenomena are introduced for the hydrostatic oscillations (Type 1 instability) that could potentially occur during ESBWR startup. The kinetics parameters are not important, as there are no reactivity feedbacks associated with these oscillations before the onset of core voiding.

The TRACG models are applicable to analyze Type 1 instabilities. At low pressure, the variations in properties with pressure along the natural circulation flow loop become important. TRACG calculates fluid properties for each node corresponding to its thermodynamic state, and therefore has the necessary capability for this purpose.

TRACG has been qualified against test data exhibiting low-pressure oscillations. TRACG Qualification for SBWR [6] includes results of comparisons with flow instability data from the CRIEPI test facility [27] (Section 6.3) and exploratory tests in the PANDA test facility (Section 6.4). The Dodewaard startup transient [29] is analyzed in Section 6.2 of the same report. No oscillations in flow were observed in the Dodewaard tests; TRACG calculated small Type 1 oscillations at the onset of void formation in the chimney. Reference 7 shows the results of comparisons between TRACG and additional CRIEPI data [30] at higher pressures of 20 and 72 bar. Table 9.2-1 shows a comparison of important non-dimensional parameters between the CRIEPI facility and the ESBWR at startup pressures. The facility was scaled to match the SBWR, and is also adequate for representing the relevant phenomena for the ESBWR. The table compares the test conditions at 2 bar with the ESBWR parameters calculated at 2 bar for the startup trajectory shown in the next section. The CRIEPI tests started at high subcooling and reduced the subcooling until Type 1 oscillations were observed. This occurred when the subcooling number and Zuber number were approximately 22. Note that the flashing number is of the order of 15 at this pressure, precluding condensation-induced oscillations ($N_{Zu} << N_{sub} + N_{fl}$). The ESBWR conditions at 2 bar are similar, with vapor generation at the top of the chimney and the subcooling numbers and Zuber numbers of the order of 22. Condensation-induced oscillations are precluded because of the large flashing number of 25. Table 9.2-2 shows a similar comparison with Dodewaard. The comparison is at 3 bar, which was the lowest pressure for which data were available from the startup of February 1992. The Zuber number and subcooling number are lower by a factor of 5 to 6 compared to ESBWR. The difference is largely due to the more favorable natural circulation characteristics of Dodewaard, which does not have separators. However, as expected, at 3 bar the Zuber number and subcooling numbers are of similar magnitude, indicating that the vapor generation is occurring in the chimney and not in the core. This was confirmed by the APRM readings that are consistent with single phase flow in the core. Note the magnitude of the margin to boiling in the core: the flashing number is three times the Zuber number. At 3 bar, the ESBWR also shows the Zuber number is beginning to exceed the subcooling number, indicating vapor generation at the top of the chimney. The Zuber number is significantly smaller than the sum of the subcooling and flashing numbers, demonstrating the margin to boiling in the core.

Tests showing condensation-induced oscillations have been reported by Aritomi et al. [26] and Kuran et al. [35]. The tests performed by Aritomi [26] have been analyzed and provide further evidence that TRACG can predict the phenomenon of condensation induced "geysering"

oscillations. However, these tests are not representative of the ESBWR geometry or startup process, and such oscillations are precluded for the range of heatup rates envisaged for the ESBWR.

Kuran et al. [35] also reported condensation-induced oscillations at low pressure. The tests were performed in a quarter-height facility. The paper describes four phases of plant startup. Phase II is "net vapor generation in the core" which occurs before Phase III "saturated chimney". The ESBWR startup is designed to avoid vapor generation in the core before the chimney region is close to saturation and until the system pressure is sufficiently high (Figure 9.1-3). This avoids the condensation-induced oscillations described in the paper. Also with the quarter-height scaling, the flashing numbers will be small relative to ESBWR, making the heatup process in the test facility more prone to condensation-induced oscillations. Finally, the reactivity feedback simulation described in the paper is of much lower consequence when voids are not generated in the core at low pressures.

Table 9.2-1:

Comparison of Non-dimensional Parameters: CRIEPI vs. ESBWR

Non-Dimensional Parameters	Typical Startup Condition (0.2 MPa)	
	ESBWR	CRIEPI
Non-dimensional downcomer cross sectional area $A_{d,e}$	1.02	1.11
Non-dimensional chimney cross sectional area A_r	2.78	2.47
Non-dimensional chimney length L_r	2.82	3.38
Ratio of vapor density to liquid density	0.0012	0.0012
Zuber Number N_{Zu}	22	21 to 25
Subcooling number N_{sub}	22	14 to 33
Flashing number N_{fl}	25	15

Table 9.2-2:

Comparison of Non-dimensional Parameters: Dodewaard vs. ESBWR

Non-Dimensional Parameters	Typical Startup Condition (0.3 MPa)	
	ESBWR	Dodewaard
Vessel L/D	3.89	4.30
Non-dimensional chimney length L_r	2.82	1.68
Ratio of vapor density to liquid density	0.0018	0.0018
Zuber Number N_{Zu}	14	2.7
Subcooling number N_{sub}	12	2.1
Flashing number N_{fl}	13	7.6

9.3 TRACG ANALYSIS OF TYPICAL STARTUP TRAJECTORIES

9.3.1 ESBWR PLANT STARTUP

Detailed startup procedures for the ESBWR will developed at a later stage. The startup process is expected to generally follow the established procedure from the Dodewaard plant. The Dodewaard plant started up for 22 cycles of operation without any problems related to flow or power oscillations.

Figure 9.3-1 shows the stages of the startup process. In the De-aeration Period, the reactor coolant is de-aerated by drawing a vacuum on the main condenser and reactor vessel using mechanical vacuum pumps with the steam drain lines open. The reactor coolant is heated up to between 80 and 90 C with the Reactor Water Cleanup/Shutdown Cooling System (RWCU/SDC) auxiliary heater (Figure 9.3-2) and decay heat. The reactor pressure is reduced to about 50 to 60 kPa. Following de-aeration, the Main Steam Isolation Valves (MSIVs) are closed to initiate the Startup Period. Control rods are withdrawn to criticality. Fission power is used to heat the reactor water, while maintaining the water level close to the top of the separators but well below the steam lines. Steaming at the free surface starts to pressurize the reactor vessel. The core region remains subcooled due to the large static head in the chimney and separators.

As the reactor heats up and pressurizes, the RWCU/SDC system heat exchangers are used to control the downcomer temperature, enhance coolant flow and reduce lower plenum stratification. The MSIVs are reopened at the end of the Startup Period, when the pressure reaches 6.3 MPa. Subsequently, the turbine bypass valves are used to control pressure. The RPV power is increased and preparations made to roll the turbine.

9.3.2 TRACG CALCULATIONS FOR SIMULATED STARTUP SCENARIOS

The startup transient for the ESBWR was simulated with TRACG. The TRACG calculations were performed with imposed core power, without activating the kinetics model. This is valid as long as there are no feedbacks from oscillations in the core void fraction during the startup transient. This assumption will be validated as part of the calculation. The calculation was initiated at the end of the de-aeration period with the steam dome pressure at 0.52 bar and RPV water at 82 C. The water level was maintained near the top of the separators. The MSIVs were closed to isolate the RPV. To simplify comparisons, the power level was maintained constant until the pressure reached 6.3MPa. Subsequently, the MSIVs were opened and the power level was increased in steps to achieve rated pressure at 300 MW (6.67% of rated power).

Three heatup rates were considered. The lowest power level of 50 MW corresponds to a heatup rate of 30 C/hour and is likely to be close to the actual value for startup. The median power level of 85 MW yields a heatup rate of 55 C/hour, which is the highest allowable to comply with reactor vessel thermal stress requirements. The highest power level of 125 MW heats up the reactor vessel water at 82 C/hour which is above allowable limits, and is only included as a sensitivity study. The three power trajectories are shown in Figure 9.3-3.

Figure 9.3-4 shows the pressure response for the three cases. The circulating water heats up because of the core power. The heat exchangers in the RWCU/SDC system are enabled to

remove a part of the energy and control the core inlet subcooling. Steam generation begins at the water surface and starts to pressurize the vessel. [[

]]

Figure 9.3-5 shows the variation in core inlet subcooling as a function of time. [[

]] The core flow transient response is shown in Figure 9.3-6. [[

]]

Further insight into the core flow response is obtained by examining the core void fractions, specifically in the highest power bundles. [[

]]

Margins to thermal limits (CPR) were calculated for the three startup scenarios. The thermal margin for the high power bundles is shown in Figure 9.3-15. Large margins are maintained throughout. Figure 9.3-16 is the corresponding plot for the peripheral bundles. Again, large margins are maintained throughout the transient. [[

]]

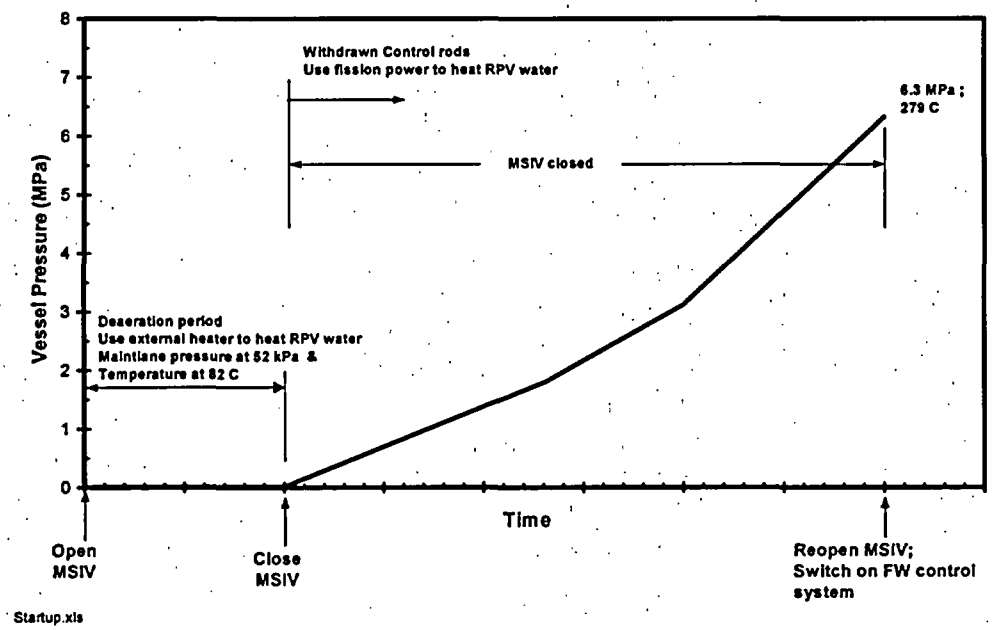

Figure 9.3-1: ESBWR Startup Trajectory

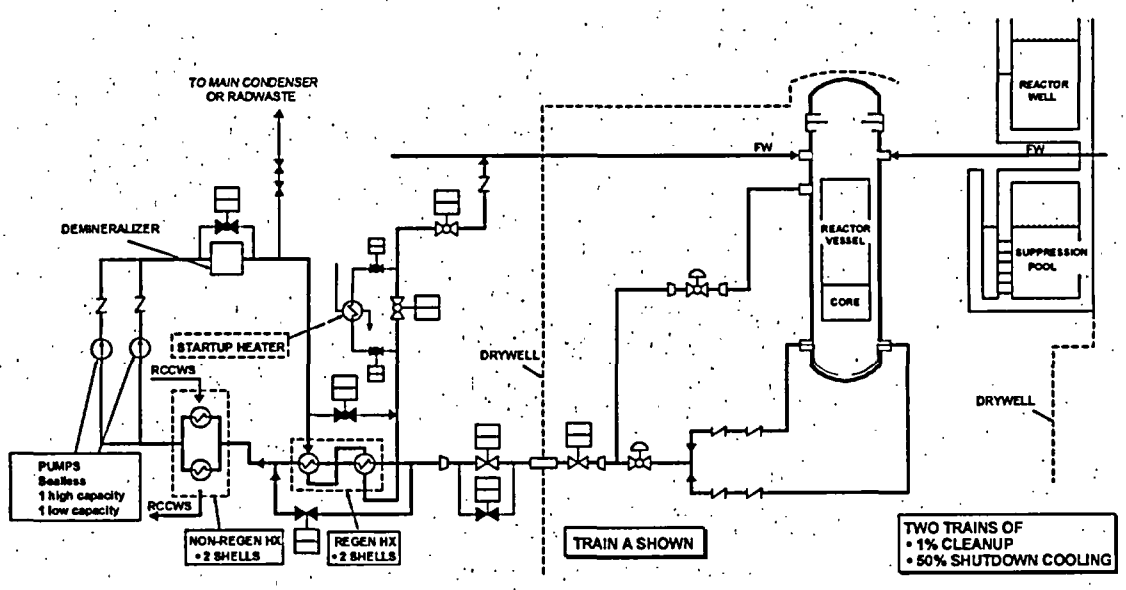

Figure 9.3-2: ESBWR Reactor Water Cleanup/Shutdown Cooling System – Schematic Diagram

[[

]]

Figure 9.3-3: TRACG Startup Simulation: Reactor Power Trajectories

[[

]]

Figure 9.3-4: TRACG Startup Simulation: Pressure Response

[[

]]

Figure 9.3-5: TRACG Startup Simulation – Core Inlet Subcooling

[[

]]

Figure 9.3-6: TRACG Startup Simulation – Core Inlet Flow

[[

]]

Figure 9.3-7: Separator Void Fraction (50 MW heatup)

[[

]]

Figure 9.3-8: Separator Void Fraction (85MW heatup)

[[

]]

Figure 9.3-9: Separator Void Fraction (125 MW heatup)

[[

]]

Figure 9.3-10: Hot Bundle Void Fraction (50 MW heatup)

[[

]]

Figure 9.3-11: Hot Bundle Void Fraction (85 MW heatup)

[[

]]

Figure 9.3-12: Hot Bundle Void Fraction (125 MW heatup)

[[

]]

Figure 9.3-13: Hot Bundle Exit Flow

[[

]]

Figure 9.3-14: Peripheral Bundle Exit Flow

[[

]]

Figure 9.3-15: Hot Bundle CPR

[[

]]

Figure 9.3-16: Peripheral Bundle CPR

9.4 SUMMARY OF ESBWR STARTUP PERFORMANCE

The TRACG simulation of ESBWR startup has demonstrated that at expected heatup rates, the startup can be accomplished without difficulty. The Type 1 instability region can be crossed with a minimum amount of flow noise. The flow noise occurred before the start of vapor generation in the core and consequently might not even be detectable on the plant power instrumentation. Thermal limits are never approached during the startup transient.

The TRACG calculations were performed without kinetics feedback. This is valid for the early part of the startup that is of interest, as there is no vapor generation in the core. TRACG calculates the condensation-induced flow oscillations observed in some experiments, but this behavior is only observed with extreme heatup rates that are well outside the range constrained by other ESBWR design considerations.

10.0 REFERENCES

[1]. J. G. M. Andersen, et al., *TRACG Model Description*, NEDE-32176P, Revision 2, December 1999.

[2]. J. G. M. Andersen, et al., *TRACG Qualification*, NEDE-32177P, Rev. 2, January 2000.

[3]. J. G. M. Andersen, et al., *TRACG Application for Anticipated Operational Occurrences Transient Analysis, NEDE-32906P-A, Revision 1*, April 2003.

[4]. GE Nuclear Energy, *General Electric Boiling Water Reactor Detect and Suppress Solution – Confirmation Density*, Licensing Topical Report NEDC-33075P, Revision 3, January 2004.

[5]. NEDE-33147: *DSS-CD TRACG Application*, February 2004.

[6]. J. R. Fitch, et al., *TRACG Qualification for SBWR*, NEDC-32725P, Rev.1, Vol.1 and 2, August 2002.

[7]. J. R. Fitch, et al., *TRACG Qualification for ESBWR*, NEDC-33080P, Rev.0, August 2002.

[8]. USNRC, *Quantifying Reactor Safety Margins: Application of Code Scaling, Applicability, and Uncertainty Evaluation Methodology to a Large-Break, Loss-of-Coolant Accident*, NUREG/CR-5249, December 1989.

[9]. USNRC, *Best-Estimate Calculations of Emergency Core Cooling System Performance*, Regulatory Guide 1.157, May 1989.

[10]. *ESBWR Design Description*, NEDC-33048P, Revision 1, August 2003.

[11]. J. G. M. Andersen, C. L. Heck and J. C. Shaug, *TRACG04 User's Manual*, GE-NE-0000-0009-7162 (UM-0136), Rev. 0.

[12]. J. S. Post and A. K. Chung, *ODYSY Application for Stability Licensing Calculations*, NEDC-32992P-A, July 2001.

[13]. GE Nuclear Energy, *BWR Owners' Group Long-Term Stability Solutions Licensing Methodology*, NEDO-31960-A, November 1995.

[14]. GE Nuclear Energy, *Steady State Nuclear Methods*, Licensing Topical Report NEDE-30130P-A, April 1985.

[15]. GE Nuclear Energy, *Qualification of the One-Dimensional Core Transient Model for Boiling Water Reactors*, Licensing Topical Report NEDE-24154P-A, August 1988.

[16]. *COLPS03A User's Manual*, UM-0133, Revision 0.

[17]. GE Nuclear Energy, *BWR Owners' Group Long-Term Stability Solutions Licensing Methodology*, NEDO-31960-A, Supplement 1, November 1995.

[18]. GE Nuclear Energy, *BWR Owners' Group Reactor Stability Detect and Suppress Solutions Licensing Basis Methodology for Reload Applications*, NEDO-32465-A, August 1996.

[19]. O. Nylund, et al., *Hydrodynamic and Heat Transfer Measurements on a Full-Scale Simulated 36 Rod BHWR Fuel Element with Non-Uniform Axial and Radial Heat Flux Distribution*, FRIGG-4, ASEA-ATOM Proprietary Report, December 1970.

[20]. P. Saha and N. Zuber, *Point of Net Vapor Generation and Vapor Void Fraction in Subcooled Boiling*, Proc. 5th International. Heat and Mass Transfer Conference., Tokyo, Japan, 1974.

[21]. S. O. Akerlund, et al., The GESTR-LOCA and SAFER Models for the Evaluation of the Loss-of-Coolant Accident, Vol.1, *GESTR-LOCA – A Model for the Prediction of Fuel Rod Thermal Performance*, NEDE-23785-1-PA, June 1984.

[22]. *Supplemental Information for Plant Modifications to Eliminate Significant In-Core Vibrations*, NEDE-21156, January 1976

[23]. L. A. Carmichael and R. O. Niemi, *Transient and Stability Tests at Peach Bottom Atomic Power Station Unit 2 at End of Cycle 2*, EPRI-NP-564, June 1978.

[24]. B. S. Shiralkar and Y. K. Cheung, *TRACG Application to ESBWR*, NEDC-33083P, November 2002.

[25]. J. March-Leuba and E. D. Blakeman, *A Mechanism for Out-of-Phase Instabilities in Boiling Water Reactors*, Nucl. Sci. Eng., Vol. 107, p. 173, 1991.

[26]. M. Aritomi, J. H. Chiang. M. Mori, *Fundamental Studies on Safety-Related Thermal-Hydraulics of Natural Circulation Boiling Parallel Channel Flow System under Startup Conditions (Mechanism of Geysering in Parallel Channels),* Nuclear Safety, Vol. 33, No.2, pp. 170-182, 1992.

[27]. F. Inada, Y. Yasuo, *The Boiling Flow Instability of a Natural Circulation BWR with a Chimney at Low Pressure Startup*, Proc. International Conference on the Design and Safety of Advanced Nuclear Power Plants (ANP '92), Tokyo, Japan, Paper 25.3, October 25-29, 1992.

[28]. T.H.J.J. van der Hagen, Personal communication, 2004.

[29]. T.H.J.J. van der Hagen, F.J. van der Kaa, J. Karuza, W.H.M. Nissen, A.J.C. Stekelenburg, J.A.A. Wouters, *Startup of the Dodewaard Natural Circulation Boiling Water Reactor,* GKN Report 92-017/FY/R, 1992.

[30]. M. Furuya et al., *Two-Phase Flow Instability in a Boiling Natural Circulation Loop at Relatively High System Pressure*, Proc. 8th International Meeting on Nuclear Reactor Thermal-Hydraulics, Vol. 3, pp. 1778-1784, Kyoto, Japan, 1997.

[31]. F. T. Bolger and M. A. Holmes, *TRACG Application for ATWS Overpressure Transient Analysis*, NEDE-32906P, Supplement 1-A, November 2003.

[32]. H. Glaeser and R. Pochard, *Review on Uncertainty Methods for Thermal Hydraulic Computer Codes*, International Conference on New Trends in Nuclear System Thermohydraulics Proceedings, Volume I, pp. 447-455, Pisa, Italy, 1994.

[33]. H. A. David, Order Statistics (2nd edition), John Wiley & Sons, New York, 1969.

[34]. D. C. Montgomery, Introduction to Statistical Quality Control, John Wiley and Sons, Inc., 1996.

[35]. S. Kuran, M. Ishii, X. Sun, L. Cheng, Y. Xu, H. Yoon, S.T. Revankar, *Nuclear Coupled Flow Instability Study for Natural Circulation BWR Startup Transient,* Paper N6P002, 6th International Conference on Nuclear Thermal Hydraulics, Operation and Safety (NUTHOS-6), Nara, Japan, October 2004,